Cerium oxide Nanoparticles: Their Phosphatase Activity and its Control

2014

Atul Dhall
University of Central Florida

CERIUM OXIDE NANOPARTICLES: THEIR PHOSPHATASE ACTIVITY AND ITS CONTROL

by

ATUL DHALL
B.E. Biotechnology, Manipal Institute of Technology, 2012

A thesis submitted in partial fulfillment of the requirements
for the degree of Master of Science in Biotechnology
in the Burnett School of Biomedical Sciences
in the College of Medicine
at the University of Central Florida
Orlando, Florida

Summer Term
2014

Major Professor: William T. Self

ABSTRACT

Cerium oxide nanoparticles are established scavengers of reactive oxygen and nitrogen species. They have many potential biomedical applications that depend on their physicochemical properties and mode of preparation. Recent studies have found these nanoparticles possess phosphatase mimetic activity. Studying such catalytic activities will qualify their biomedical applications and render information on their bioavailability and potential toxicity.

Two oxidation states of cerium exist in these nanoparticles (3+ or 4+). It is hypothesized that the oxidation state of cerium in the nanoparticles determines the amount of adsorbed water on the crystal lattices. This in turn governs their activity as phosphatases. Nanoparticles with higher levels of cerium in the 4+ state exhibit phosphatase activity while those with higher levels of cerium in the 3+ state do not. This phosphatase activity may be controlled with the addition of inhibitory anions. It is hypothesized that anions with structures similar to phosphate can inhibit phosphatase activity by leading to the production of complexes on the surface of cerium oxide nanoparticles.

Substrates that were used to test this activity include para-nitrophenyl phosphate (pNPP), 4-methylumbelliferyl phosphate (MUP) and adenosine triphosphate (ATP). To highlight the role of adsorbed water, we also performed experiments on pNPP with methanol as a solvent. The activity was measured by absorbance (pNPP and ATP) or fluorescence (MUP) and reported as nmol of phosphate/min. In some cases this rate was calculated through coupled reactions or by measuring the rate of formation of other colored products formed along with the release of phosphate such as pNP (para-nitrophenol).

The phosphatase activity increased as the amount of adsorbed water increased implying that the abundance of adsorbed water makes the surface of 4+ ceria nanoparticles more active. Phosphatase activity for all the substrates exhibited Michaelis-Menten kinetics. Although the phosphatase activity of these nanoparticles is slow (turnover rate) as compared to real biological phosphatases, it can be used as a model catalytic activity to follow other catalytic activities that are associated with nanoparticles that have an abundance of cerium in the 4+ state, such as catalase activity. These results also provide information on the nature of the active sites involved in the catalytic activities associated with these nanoparticles.

We identified three inhibitors, tungstate, molybdate and arsenate, which decreased the phosphatase activity of these nanoparticles in a dose dependent manner. V_{max}, K_m and K_i values were determined by varying substrate concentrations in the presence and absence of inhibitors. A partial mixed inhibition model was fit for each of these inhibitors.

Summary: Phosphatase activity of cerium oxide nanoparticles with higher levels of cerium in the 4+ oxidation state was used as a model catalytic activity to study the nature of the active sites involved in catalysis. The study of inhibitors can reveal more information as to the surface binding of substrates in catalysis.

ACKNOWLEDGMENTS

This project would not have been possible without the financial support provided by grants from the National Science Foundation (NSF- CBET 0930170 and CBET 0708172). Firstly, I would like to thank Dr. Janet Dowding for her constant guidance throughout the course of this project. She helped me settle into a completely new work environment and also aided in the setting up of my thesis proposal. Secondly, I would like to thank Dr. Soumen Das for providing our lab with cerium oxide nanoparticles that were used throughout this project. He also helped me with experiments that involved the use of Dynamic Light Scattering and X-Ray Photoelectron Spectroscopy. I would also like to thank Rameech McCormack for analyzing the data from X-Ray Photoelectron Spectroscopy experiments.

I am grateful to my thesis committee members, Dr. Sudipta Seal and Dr. Antonis Zervos, and the graduate coordinator for M.S. students, Dr. Saleh Naser, for their constant support and guidance. Finally, I would like to thank my committee chair, Dr. William Self for all his help during the last two years. He was incredibly patient and always had words of encouragement.

TABLE OF CONTENTS

LIST OF FIGURES

LIST OF TABLES

LIST OF ACRONYMS

AIC: Akaike Information Criterion

ATP: Adenosine triphosphate

CIP: Calf Intestinal Phosphatase (Alkaline)

CMP: Chemical Mechanical Planarization

DLS: Dynamic Light Scattering

MESG: 2-amino-6-mercapto-7-methyl purine riboside

MUP: 4-methylumbelliferyl phosphate

PNP: purine nucleoside phosphorylase

pNP: para-nitrophenol

pNPP: para-nitrophenyl phosphate

XPS: X-Ray Photoelectron Spectroscopy

LIST OF SYMBOLS

E: Enzyme

I: Inhibitor

K_i: Equilibrium Dissociation constant (Inhibitor)

K_p: Equilibrium Dissociation constant (Product)

K_s: Equilibrium Dissociation constant (Substrate)

K_m: Michaelis-Menten constant

P: Product

S: Substrate

v: Initial rate of reaction

V_{max}: Maximum rate of reaction

α: Inhibition constant for inhibitory path followed

β: Inhibition constant for degree of inhibition

INTRODUCTION

In a report by the US National Science and Technology Council [1] we come across a rather simple definition for nanotechnology.

"The essence of nanotechnology is the ability to work at the molecular level, atom by atom, to create large structures with fundamentally new molecular organization. The aim is to exploit these properties by gaining control of structures and devices at atomic, molecular, and supramolecular levels and to learn to efficiently manufacture and use these devices."

Most working definitions of nanotechnology tend to limit nanomaterials as having at least one dimension between 1-100nm. The breakdown of larger objects into smaller objects offers two distinct advantages. Firstly, the number of such objects increases. If the task at hand requires individual objects to perform a certain function then the more of these objects we have, the more efficient the functioning of the system will be. Secondly, the surface area of the objects increases. If the task at hand requires active contact with objects, then the greater the area available for contact, the quicker the process will be.

These advantages stay intact when we are dealing with biological systems. However, a crucial third advantage almost overshadows the first two. Biological environments consist of molecules, especially proteins that interact at the nanometer level. This means that the nano-world we have stumbled upon in the past few decades has in fact been operational from the very beginning of life. If we engineer nanomaterials that fit the dimensions of molecular biology, then we give

ourselves a much better chance of interaction with this nano-world. Nanobiotechnology then simply refers to the use of nanotechnology to study biological systems.

Cerium Oxide Nanoparticles

Cerium oxide is a rare-earth oxide of the lanthanide series. It has an established role in the polishing industry but its applications in the biomedical industry have only recently been discovered. Cerium oxide nanoparticles exist with two oxidation states for cerium - 3+ and 4+. While they have been shown to possess certain enzyme mimetic activities, the exact chemical nature of the active sites of these nanoparticles is still unclear. The toxicity of these nanoparticles is also under debate. Since the bioavailability, toxico-kinetics and toxico-dynamics of nanoparticles are influenced by their physicochemical characteristics [2], we have used the phosphatase mimetic activity of cerium oxide nanoparticles as a model catalytic activity. The knowledge gained will help qualify their biomedical applications. It will also provide an insight on the chemical nature of the active sites involved during catalysis.

To study the size and oxidation state of the cerium oxide nanoparticles, we have utilized three methods – Dynamic Light Scattering (DLS), UV-Visible Spectroscopy and X-Ray Photoelectron Spectroscopy (XPS). Very briefly, DLS is a routine technique used to estimate the particle size of small particles in solution. It is based on the principle that small particles in solution undergo Brownian motion and will scatter light in a manner that fluctuates with time. The scattered light can then interfere (either constructively or destructively) and can be used to generate data on the movement of particles with respect to time.

XPS is a technique that can be used to study the elemental composition of a sample and investigate the state of the atoms in that sample. Figure 1 provides a simple schematic for XPS.

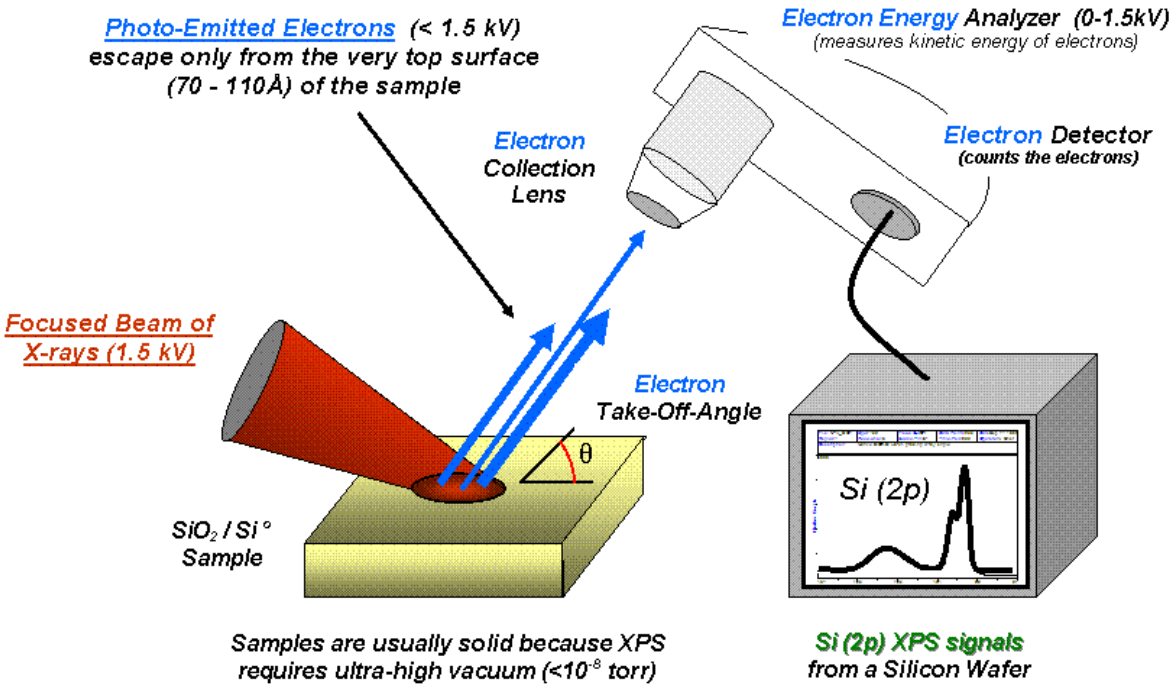

Figure 1: A schematic of X-Ray photoelectron spectroscopy
This image is available in the public domain as a part of Wikimedia Commons:
http://en.wikipedia.org/wiki/X-ray_photoelectron_spectroscopy#mediaviewer/File:System2.gif

Samples are irradiated with a beam of X-rays under ultra-high vacuum. The binding energy and number of electrons that escape from the surface is measured and displayed as a spectrum. This when compared to standard spectra for known elements can help us derive the elemental composition of the sample and the state of the atoms that are present in the sample.

Major Aims of this Project

The first aim of this project was to investigate the mechanism of phosphatase activity of cerium oxide nanoparticles. A suitable mechanism was proposed based on similarity to established models of enzyme kinetics. Several preparations of cerium oxide nanoparticles were tested to correlate material properties to catalytic efficiency.

The second aim of this project was to highlight the role of water in the hydrolytic chemistry involved during removal of phosphate groups from donor substrates. A clear relationship between the amount of water required for catalysis and the rate of phosphatase activity was established.

The final aim of this project was to establish the role of inhibitory anions in controlling the phosphatase activity of cerium oxide nanoparticles. Dose dependent in vitro assays were conducted to establish the nature of these inhibitors. Multiple substrates were used to rule out potential artifacts that might occur in these chemical reactions.

Phosphatase Activity

Throughout the course of this project we used both artificial substrates such as para-nitrophenyl phosphate (pNPP) and 4-methylumbelliferyl phosphate (MUP) as well as bio-relevant substrates (ATP) to measure the phosphatase activity of cerium oxide nanoparticles. Reasons for choosing this activity include the simplicity of measurement and the fact that it can be used as a model for other key catalytic activities of cerium oxide nanoparticles.

Enzyme Inhibition

Models for enzyme inhibition are now well established and software can use standard models to generate kinetic parameters for given experiments. Figure 2 provides a simple schematic for the different routes in a single substrate reaction.

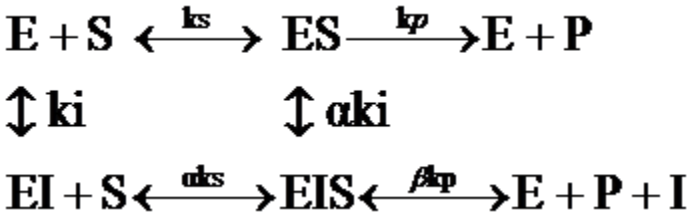

Figure 2: Different routes in enzyme inhibition

E is used to denote the Enzyme. The symbols S, P and I are used for the Substrate, Product and Inhibitor respectively. K with different subscripts is used to denote the dissociation constant for each reaction. The symbols α and β represent constants that are used to classify the type of the inhibition. While α helps distinguish models based on type of complex formed, β helps distinguish between full and partial inhibition of the reaction. Table 1 summarizes the different types of enzyme inhibition and the routes followed.

Table 1: Different types of enzyme inhibition

TYPE OF INHIBITION	PATH FOLLOWED
Competitive	I binds to only E
Mixed	I binds to both E and ES
Non-Competitive (Special Mixed)	I binds to both E and ES with equal affinity
Uncompetitive	I binds to only ES

The Michaelis-Menten model for enzyme kinetics is a common model for most basic enzymatic reactions. The phosphatase activity of cerium oxide nanoparticles also follows Michaelis-Menten kinetics. The model is described by the following equation.

$$v = \frac{\mathrm{Vmax}.[\mathrm{S}]}{\mathrm{Km} + [\mathrm{S}]} \quad (1)$$

Where v is the initial rate of the reaction, V_{max} is the maximum rate of the reaction, K_m is the Michaelis-Menten constant and S is the Substrate. Since this does not produce a linear plot, the equation is often modified to the double reciprocal plot or Lineweaver-Burk equation. The equation is as follows.

$$\frac{1}{v} = \frac{K\mathrm{m}}{V\mathrm{max}.[\mathrm{S}]} + \frac{1}{V\mathrm{max}} \quad (2)$$

This equation is linear and thus makes calculation of kinetic parameters easier. One example of a model for enzyme inhibition is partial mixed inhibition. This model encompasses all possible routes that the reaction can follow and thus Figure 2 is an apt schematic for it. The rate of reaction for this model is given by the following equation.

$$v = \frac{V\mathrm{max}.[\mathrm{S}](1+\beta)}{K\mathrm{s}\left(1+\frac{[\mathrm{I}]}{K\mathrm{i}}\right)+[\mathrm{S}](1+\frac{[\mathrm{I}]}{\alpha.\ K\mathrm{i}})} \quad (3)$$

Since β involves a second route for the product to form it makes sense that it is in the numerator. The constant α on the other hand, is involved in the formation of EIS complex and thus should be part of the denominator. It is quite easy to note that equation 3 is derived from equation 1.

Phosphatases in Biology

Simply put, a phosphatase is an enzyme that removes a phosphate group from a donor substrate with the help of water. This means that they act in direct opposition to kinases and phosphorylases.

Alkaline phosphatases are the most common type in biological environments. Kinases along with phosphatases are integral to many signal transduction pathways. This is because proteins are activated and deactivated by the addition and removal of phosphate groups. Additionally phosphatases such as Calf Intestinal Phosphatase (CIP) are useful in removal of phosphorylated ends of DNA and RNA. This allows end-labeling of probes. One of the experiments in this project involved comparing the phosphatase activity of CIP with that of cerium oxide nanoparticles.

Addition or removal of phosphate groups is also vital in energy maintenance because it pertains to the energy storage molecule, ATP. ATP cleaves into ADP and inorganic phosphate and releases energy while doing so. This energy is then used to carry out all kinds of cellular functions. Thus there is a need to maintain a fine balance for ATP levels in order to control metabolic activities. Nanoparticles that can alter ATP levels may disrupt this fine balance and hence be toxic. Studying the ATPase activity of cerium oxide nanoparticles will provide us with information on their toxicity.

LITERATURE REVIEW

This chapter begins with a brief overview of the structural properties of cerium oxide and their known catalytic activities. It then continues to the applications of cerium oxide nanoparticles in the biomedical industry. Finally a few industrial applications are discussed.

Structural Properties of Cerium Oxide Nanoparticles

Cerium exists in two oxidation states in cerium oxide nanoparticles – 3+ and 4+. The most common deviations from the regular structure of the stoichiometric surface (found in bulk cerium oxide) are surface oxygen vacancies (due to an increased amount of 3+), water adsorbed on top of cerium ions and hydroxide substituting surface oxygen [3]. Dynamic scanning force microscopy has been used to study the adsorption of water molecules on a stoichiometric CeO_2 (111) surface at room temperature. It is suggested that water molecules localize exclusively on this type of site that is associated with the cerium-ion sub-lattice and stick to the surface with an estimated surface diffusion barrier of 1eV [4].

A recent report suggests that cellular interactions and toxicity of these nanoparticles depend on their physicochemical properties and surface modifications[5]. The presence of Ce^{3+} implies the defect structure $Ce0_{2-x}$ for ceria nanoparticles due to oxygen vacancies. Figure 3 shows a 3D model of the cerium oxide lattice. Cerium atoms are shown in red while oxygen atoms are off-white. Oxygen vacancies are introduced during the synthesis of cerium oxide nanoparticles and can be thought as one of the off-white atoms popping out from the lattice. This lends an overall CeO_{2-x} structure to the lattice. The transformation of ceria 4+ to 3+ plays a vital role in the catalytic properties of ceria [6].

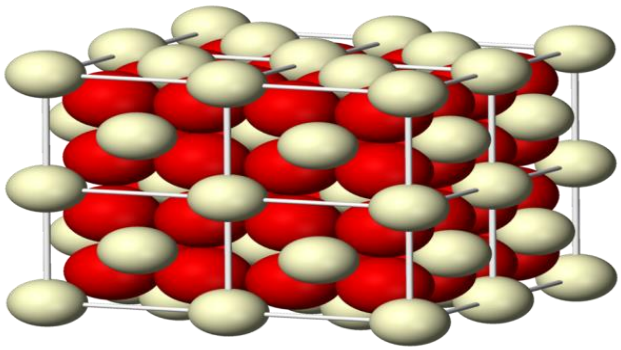

Figure 3: Overall $Ce0_{2-x}$ structure of lattice
This image is available in the public domain as a part of Wikimedia Commons: http://en.wikipedia.org/wiki/File:Ceria-3D-ionic.png

The surface reactivity of cerium oxide nanoparticles is critically dependent upon the nature of the environment in which they reside. Simulations predict higher activities of ceria nanoparticles, towards oxygen release, when immersed in water. Atomistic simulations though, inherently do not account for the biological environment surrounding these nanoparticles. Molecular simulations, on the other hand, are more realistic in predicting their surrounding environment. Figure 4 [7] shows surface rendered models of cerium oxide nanoparticles crystallized in water. The surface is colored according to calculated electrostatic potential revealing reactive (red) compared to unreactive (blue) regions on the nanoparticle. 4(b) is as 4(a) but after removal of water and system minimization.

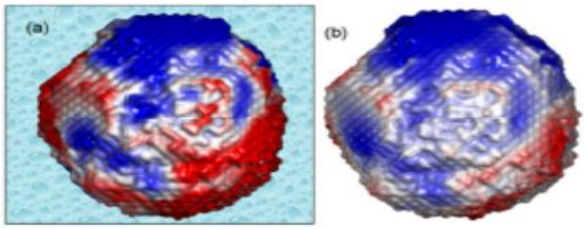

Figure 4: Surface rendered models of cerium oxide nanoparticles
Reproduced from [7] with permission of The Royal Society of Chemistry.

Nanoparticles with high 3+/4+ ratio show minimal phosphatase activity while those with a low 3+/4+ ratio show significant phosphatase activity. Removal of phosphate groups from both artificial substrates such as pNPP or MUP, and bio-relevant substrates such as ATP, is thought to involve hydrolytic chemistry.

ROS/RNS Scavenging and Enzyme Mimetic Activities

Cerium oxide nanoparticles have been shown to scavenge nitric oxide [8] and superoxide radicals [9]. Nanoparticles with ceria predominantly in the 4+ state are better at scavenging nitric oxide radicals while those with a 3+ state predominance can scavenge superoxide radicals more efficiently [8]. A review article in 2010 [10] expounds the role of cerium oxide nanoparticles in effectively protecting mammalian cells. They have also been shown to significantly alter the rate of decay of peroxynitrite [11] as well as exhibit catalase mimetic activity in the 4+ state [12].

Some studies have indicated a more toxic nature, *i.e.*, cerium oxide nanoparticles can generate reactive oxygen species depending on certain crucial factors such as buffer anions [13]. The report defines the effects of different buffer anions by using Tris-HCl, sulfate, and phosphate buffer solutions and illustrates their DNA protective effect. The results indicate that cerium oxide nanoparticles can protect DNA from damage in Tris-HCl and sulfate systems, but not in phosphate buffer solution systems. Cerium phosphate formed on the surface of the nanoparticles, interferes with the redox cycling between Ce^{3+} and Ce^{4+}.

Table 2 is drawn from information reported in two studies [5, 11] and shows the various bio-catalytic properties of Ce^{3+} and Ce^{4+}.

Table 2: Bio-catalytic activities of cerium oxide nanoparticles

CATALYTIC ACTIVITY	Ce^{3+}	Ce^{4+}
Phosphatase[a]	No	Yes
·NO scavenger[a]	No	Yes
Catalase mimetic[a]	No	Yes
SOD mimetic[a]	Yes	No
Peroxynitrite scavenger[b]	Yes	Yes

Superscript 'a' represents data taken from [5] while 'b' represents data taken from [11].

A report in 2011 [14] suggests that cerium oxide nanoparticles are resistant to broad changes in pH and are unaltered by incubation in cell culture medium. However, phosphate anions significantly alter their characteristics and shift the catalytic behavior when incubated in phosphate buffer. Therefore it is speculated that the local concentration of phosphate anions in cells can greatly affect the catalytic properties of nanoparticles.

Other Biomedical Applications

Commercial availability of cerium oxide nanoparticles makes it extremely likely that they will be introduced into the environment. This validates the need to gather knowledge of their fate, transport and bioavailability in natural aquatic systems [2]. Characterizing the environmental transport and quantifying the risk of nanoparticles involves understanding the aggregation of nanoparticles [15].

PEGylation of the surface provides stealth characteristics to nanoparticles so that they are not identified as foreign materials by the human body [16]. Cerium oxide nanoparticles have been

shown to trigger angiogenesis by modulating the intracellular oxygen environment and stabilizing hypoxia inducing factor 1alpha (HIF-1α) endogenously [17]. In addition, nanocomposite scaffolds of bioactive glass foams containing tailor made nanoceria additives have been shown to enhance the production of collagen by HMSCs [18].

Industrial Applications

Industrial applications of cerium oxide take advantage of cerium's high thermodynamic affinity for oxygen and sulfur and the unique absorption/excitation energy bands associated with its electronic structure [19]. Most activities of cerium oxide nanoparticles work on the shuttling between cerium in 3+ and 4+ states.

Slurries of cerium oxide have traditionally been used in glass polishing. Cerium oxide nanoparticles are currently also used as an abrasive for chemical-mechanical planarization (CMP) of integrated circuits [20]. CMP is a technique used to smoothen out surfaces using chemical and mechanical forces. In nanoelectronics, it is used to connect individual transistors on a chip. This is incredibly useful for mass-manufacturing of chips for nanoelectronics as it gets rid of a majority of polishing defects.

The slurry for CMP usually contains particle-based abrasives. Spherical nanoparticles are ideal polishing agents because they can act like ball bearings and reduce the scratching of surfaces [20]. The exact polishing mechanism using ceria based slurries remains unclear but Suphantharida *et al.* [21] implicate that the adsorption of silicate ions on ceria may be necessary for the removal mechanism of silicon-based materials in the CMP technique.

Cerium oxide nanoparticles are also used in water-gas shift catalysis, combustion catalysis, oxygen ion conductors, solid oxide fuel cells [22] and in electrochromic thin films [23].

METHODOLOGY

This chapter starts off with a description of the method used to prepare cerium oxide nanoparticles. It goes on to describe the methods used to characterize the nanoparticles. Subsequently, a detailed methodology for the various assays to check phosphatase activity is provided. The assays are described in an order that matches the aims described in the introduction. Finally the methodology adopted for comparing phosphatase activity of cerium oxide nanoparticles to that of CIP is described.

Preparation of Cerium Oxide Nanoparticles

This project utilized two preparations of cerium oxide nanoparticles – one with a high Ce^{3+}/Ce^{4+} ratio and one with a low Ce^{3+}/Ce^{4+} ratio. All nanoparticles that were used in this project were prepared by the same wet chemical method described by Das *et al.* [17]. The precursor used was cerium nitrate hexahydrate (99.999% pure from Sigma Aldrich, St. Louis, MO). The precursor was dissolved in distilled water and stoichiometric amounts of H_20_2 (for high Ce^{3+}/Ce^{4+} ratio) or NH_4OH (for low Ce^{3+}/Ce^{4+} ratio) were added. The resulting solutions for each case were mixed thoroughly. The NH_4OH solution was washed four times with double distilled water and resuspended in the same volume of water. The pH of these solutions was adjusted to 3 to maintain stable suspensions. Surface modified cerium oxide nanoparticles were prepared using hexamethylenetetramine (HMT) [24]. This sample was called HMT-ceria. For convenience, nanoparticle solutions with a high Ce^{3+}/Ce^{4+} ratio are labeled as 3+ while those with a low Ce^{3+}/Ce^{4+} ratio are labeled as 4+. This does not imply the lack of one state in a preparation. Instead it seeks to identify the dominant state in each preparation. It is important to note that the

precursor was originally at 5mM and so the resulting solution's cerium concentration was also 5mM. This does not equate to the concentration of cerium oxide nanoparticles. There are thousands of cerium atoms in a nanoparticle and the actual concentration of the active sites at the surface of these nanoparticles is unclear. The subsequent sections mention values for the nanoparticle concentration. These values actually refer to the cerium concentration in these nanoparticles.

Characterization of Cerium Oxide Nanoparticles

The consistency between different batches of nanoparticles for size was confirmed by DLS measurements. The Zetasizer Nano ZS (Malvern Instruments, Worcestershire, UK) was used to measure the size of different batches of 4+ nanoparticles at $[Ce^{4+}]$ = 250µM. Size was calculated before and after 5 minutes of ultrasonication of the samples in 1 ml cuvettes.

The consistency in Ce^{3+}/Ce^{4+} ratio was confirmed by observing the similarity in the UV-Visible spectra of different batches. An Agilent 8453 (HP) UV-Vis Spectrophotometer (Agilent Technologies, Santa Clara, CA, USA) was used to measure the spectra of 4+ and 3+ nanoparticles at 125µM. 50µl of sample was placed in a quartz spectrophotometer cell (Starna Cell, Inc., Atascadero, CA, USA) and both UV and visible lamps were switched on to observe the spectra from 200-900nm.

The state of cerium oxide nanoparticles with and without inhibitory anions (tungstate, molybdate and arsenate) was observed by a PE-PHI-5400 X-Ray Photoelectron Spectrometer (Physical Electronics, Chanhassen, MN, USA). 15µl each of 5mM nanoparticle solution and 5mM inhibitor solution were mixed and applied to silicon wafers. The wafers were allowed to dry and

the process was repeated 6 times till a distinct film of the sample was visible on the wafers. Samples were then loaded with the assistance of the staff at the Material Characterization Facility AMPAC of the University of Central Florida. Samples were aligned to maximize signal and then a survey was performed to check the contents of the sample. Subsequently, XPS spectra for the elements in question were obtained for at least 3 cycles with at least 5 sweeps. Spectra for cerium 3d orbitals were generated and the Ce^{3+} concentration was reported.

Phosphatase Activity of Cerium Oxide Nanoparticles

The phosphatase activity of cerium oxide nanoparticles was detected using four different assays that used different phosphate donors as substrates. Methods of detection included absorbance and fluorescence. The substrates used were - pNPP and MUP (artificial) and ATP (bio-relevant).

Mechanism of Phosphatase Activity

The assays with artificial substrates were used to understand the mechanism of the phosphatase activity of cerium oxide nanoparticles. Initially various compounds were screened to detect phosphatase activity in the pNPP assay. Subsequently the activity of 4+ and 3+ cerium oxide nanoparticles was compared. This was followed by a series of experiments to track saturation of phosphatase activity and replenish substrate at the point of saturation. SigmaPlot® 12.5 (Systat Software, Inc., Point Richmond, CA, USA) was used to generate Michaelis-Menten curves and Lineweaver-Burk plots and it provided values for V_{max} and K_m.

pNPP Assay

The phosphatase mimetic ability of CeO_2 nanoparticles was assayed by the hydrolysis of para-nitrophenyl phosphate (New England BioLabs Inc., Ipswich, MA, USA) into para-nitrophenol,

which turns into its conjugate base, para-nitrophenolate. All tests were conducted in 96 well plates and the well volume was maintained at 200µl by adding appropriate amounts of water. HEPES at a pH of 7 and a concentration of 50mM was used as a buffer for the reaction. The reaction was followed by measuring the absorbance at 405nm (for para-nitrophenolate) using a Spectramax 190 UV-Visible spectrophotometer (Molecular Devices, Sunnyvale, CA, USA). SigmaPlot® 12.5 was used to draw normalized absorbance vs time graphs.

Screening of Various Catalysts

The substrates used were yttrium oxide, indium tin oxide, cerium oxide powder, HMT-nanoceria, cerium oxide – yttria doped, water based 4+ nanoceria and sodium hydroxide. The concentration of pNPP was maintained at 1.2mM. The reaction was followed by measuring the absorbance every minute for 20 minutes. The same procedure was followed for 4+ and 3+ cerium oxide nanoparticles at 100µM to compare their phosphatase activity.

Saturating the Catalyst and Replenishing Substrate

A similar procedure to the one just described was used to observe the time taken for the reaction to saturate using 4+ cerium oxide nanoparticles at 100µM. Two pNPP concentrations were tested – 1.2mM and 9.6mM. The reaction was followed for 60 minutes. Subsequently an experiment was conducted to replenish 1.2mM pNPP at the end of 60 minutes with the nanoparticle concentration being 200µM.

Kinetics of Phosphatase Activity

The 4+ nanoparticle concentration was fixed at 200µM. Different concentrations of pNPP were used – 0.3, 0.6, 1.2, 2.4, and 4.8mM. The experiment was conducted 3 times with triplicates in a

96 well-plate. The initial rate of the reaction from minute 1 to 6 was calculated by using the change in absorbance (Δabs/min). Average rates from each triplicate set were then used to calculate the initial rate of pNP formed in nmol/min using the molar extinction coefficient for pNPP (=18.5$mM^{-1}cm^{-1}$). The rate of phosphate formed was the same as that of pNP because of stoichiometry. V_{max} and K_m values were generated by SigmaPlot® 12.5 along with a Michaelis-Menten curve and a Lineweaver-Burk plot.

MUP Assay

To corroborate evidence, phosphatase activity of cerium oxide nanoparticles was also detected by fluorescence in the MUP assay. A 10mM stock of 4-Methylumbelliferyl phosphate (Molecular Probes Inc., Eugene, OR, USA) was made in HEPES (at pH 7). The reaction involved exciting 1mM of MUP at 360nm and detecting the fluorogenic product, 4-methylumbelliferone at 449nm. Fluorescence was detected by Varian Cary Eclipse Fluorescence Spectrophotometer (Agilent Technologies, Santa Clara, CA, USA) once every minute. The assay was performed in white round-bottomed 96 well-plates. The reaction volume was maintained at 200µl by adding water. HEPES was maintained at a concentration of 25mM and cerium oxide nanoparticles were at 200µM. The rate of phosphate formation was calculated in Δintensity/min.

The phosphatase activity of 4+ and 3+ nanoparticles was compared (followed for 20 minutes) and the time taken for the assay to saturate was observed (followed for 2 hours).

Malachite Green Assay

The phosphatase activity was further confirmed by using a bio-relevant substrate. The phosphatase activity of CeO_2 nanoparticles was assayed by the hydrolysis of ATP (Sigma

Aldrich, St. Louis, MO, USA) using the Malachite Green phosphate detection kit (RnD Systems, Minneapolis, MN, USA). HEPES at a pH of 7 and a concentration of 50mM was used as a buffer in the reaction. All tests were conducted in 96 well plates and water was used to bring the reaction volume to 100µl. The nanoparticle concentration was 200µM while the concentration of ATP was varied between 0 and 200µM. Volumes of ATP were added at different intervals for a 30 minute period to simulate a kinetically followed reaction. 20µl each of Reagent A, with 10 minutes of incubation, and Reagent B, with 20 minutes of incubation, were used as reaction stopping agents and they produced the chromogenic product to be measured at 620nm. End-point absorbance was measured at 620nm using a Spectramax 190 UV-visible spectrophotometer. A phosphate standard from the kit was used to enable the establishment of standard curve that related the absorbance to nmol of phosphate per well.

EnzChek® Phosphate Assay

A second assay was used to confirm activity for a bio-relevant substrate. The phosphatase mimetic activity of CeO_2 nanoparticles was assayed by the hydrolysis of ATP using the EnzChek® Phosphate Assay Kit (Molecular Probes Inc., Eugene, OR, USA). In the presence of P_i, the substrate 2-amino-6-mercapto-7-methyl purine riboside (MESG) is enzymatically converted by purine nucleoside phosphorylase (PNP) into ribose 1-phosphate and 2-amino-6-mercapto-7-methylpurine. This conversion can be followed at 360nm. UV transparent 96 well-plates were used. The concentration of nanoparticles was 200µM while that of ATP was 100µM. The reaction was followed (after 10 minutes of incubation) for 30 minutes at one minute intervals using a Spectramax 190 UV-visible spectrophotometer. Phosphate standard from the kit

was used to derive a standard curve that related the absorbance to nmol of phosphate per well. SigmaPlot® 12.5 was used to draw a graph of phosphate formed (nmol/well) vs time.

Role of Water in Phosphatase Activity

The role of water in the phosphatase activity of cerium oxide nanoparticles was studied by replacing water with methanol in steps of 10% of the reaction volume (20-120µl). Experiments were conducted only for the artificial substrates (pNPP and MUP).

The general strategy for these assays was the same as described above. Nanoparticle concentrations were kept at 200µM. The actual concentration of water in the reaction was calculated by using percentages of 55.55M and working backwards serially. For the pNPP assay, the initial rate of pNP formed was calculated in nmol/min. The concentration of pNPP was 1.2mM. For the MUP assay, rates were left in Δintensity/min. The concentration of MUP was 500µM. SigmaPlot® 12.5 was used for both assays to draw a graph of rate of reaction in nmol/min or Δintensity/min vs water concentration (M).

Inhibition of Phosphatase Activity

Preliminary experiments were conducted with sodium salts of sulfate, selenate, tungstate, arsenate and molybdate. Kinetic parameters were found for the anions that were able to inhibit phosphatase activity (tungstate, molybdate and arsenate).

pNPP Assay

Concentration of the inhibitory salts used were [I] = 0.2, 0.5 and 1mM. After choosing the anions that inhibited phosphatase activity (tungstate, molybdate and arsenate), kinetic studies were

performed over [pNPP] = 0.3, 0.6, 1.2, 2.4 and 4.8mM and [I] = 0, 0.15, 0.3 and 1.8mM. Rates were calculated in nmol/min using molar extinction coefficient for pNPP (=18.5$mM^{-1}cm^{-1}$). The experiments were conducted 3 times with triplicates in a 96 well-plate. The Enzyme Kinetics wizard of SigmaPlot® 12.5 was used to test different models of enzyme inhibition. Models were fit to the data and ranked according to their R^2 values. The Akaike Information Criterion (AIC) is used to compare non-nested models of enzyme kinetics. It deals with the trade-off between the goodness of fit of the model and the complexity of the model. AICc refers to the same criterion with a correction for finite sample sizes. This means that there is a greater penalty for extra parameters. Secondary consideration was given to their AICc values while choosing a model for inhibition. Michaelis-Menten curves and Lineweaver-Burk plots were generated for all the models. Values of V_{max}, K_m, K_i, α and β were generated for the chosen model.

MUP Assay

To corroborate evidence from pNPP assays, inhibition of phosphatase activity of cerium oxide nanoparticles was also detected by fluorescence in the MUP assay. The reaction involved exciting 0.5mM of MUP at 360nm and detecting the fluorogenic product, 4-methylumbelliferone at 449nm. Inhibitor concentrations used were 25, 50, 100 and 200µM. Fluorescence was detected in the same manner as described previously. The reaction volume was maintained at 200µl by adding water. HEPES was maintained at a concentration of 25mM and cerium oxide nanoparticles were at 200µM.

Malachite Green Assay

The inhibition of phosphatase activity was further confirmed by using a bio-relevant substrate. The nanoparticle concentration was maintained at 200µM while the concentration of ATP was varied between 0 and 200µM. The inhibitor concentration was also varied between 0 and 200µM. The rest of the experiment was conducted as described above.

EnzChek® Phosphate Assay

A second assay was used to confirm activity for a bio-relevant substrate. The concentration of nanoparticles was maintained at 200µM while that of ATP was 50µM. Inhibitor concentrations used were 100 and 200µM. The rest of the experiment was conducted as described above.

Phosphatase Activity of Biological Phosphatase

Alkaline Phosphatase - Calf Intestinal (New England BioLabs® Inc., Ipswich, MA, USA) was used as a comparison for the phosphatase activity of cerium oxide nanoparticles. Experiments were conducted with pNPP at 1.2mM and in CutSmart™ buffer at 37ºC. The reaction was followed for 7 minutes at 405nm using the same technique as described previously. The enzyme formulation had a concentration of 3.33mg/ml (10000U/ml with specific activity of 3000U/mg). This was treated as 47.83µM as the theoretical molecular weight of the protein was 69kDa. By trial and error a value for enzyme volume was found such that change in absorbance with time is roughly the same for both enzyme and nanoparticles. This value represented a final enzyme concentration of about 570nM in the 200µl reaction well.

Experiments were conducted in triplicate with and without 0.3mM of inhibitors (tungstate, molybdate and arsenate). As a comparison, 4+ cerium oxide nanoparticles at 200µM were used in the same environment to demonstrate their phosphatase activity.

RESULTS AND DISCUSSION

This chapter discusses the results for the various experiments described in the methodology section. The order in which these results are described matches the aims of this project. Each figure is followed by its discussion.

Size of 4+ Nanoparticles

The size of 4+ nanoparticles used was confirmed by DLS measurements before and after ultrasonication. Different batches of 4+ and 3+ nanoparticles were tested to examine consistency in their spectra. Figure 5 and 6 show the size distribution of 4+ nanoparticles before and after ultrasonication respectively.

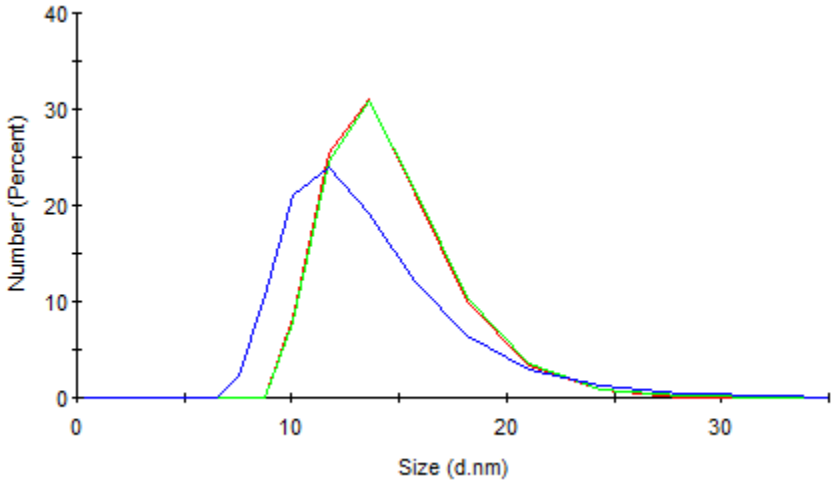

Figure 5: 4+ nanoparticles are between 10-20nm in size before ultrasonication
Size was measured by DLS before ultrasonication. [Ce^{4+}] = 250µM. Each color represents a replicate of the same sample. Size was measured 11 times for each replicate.

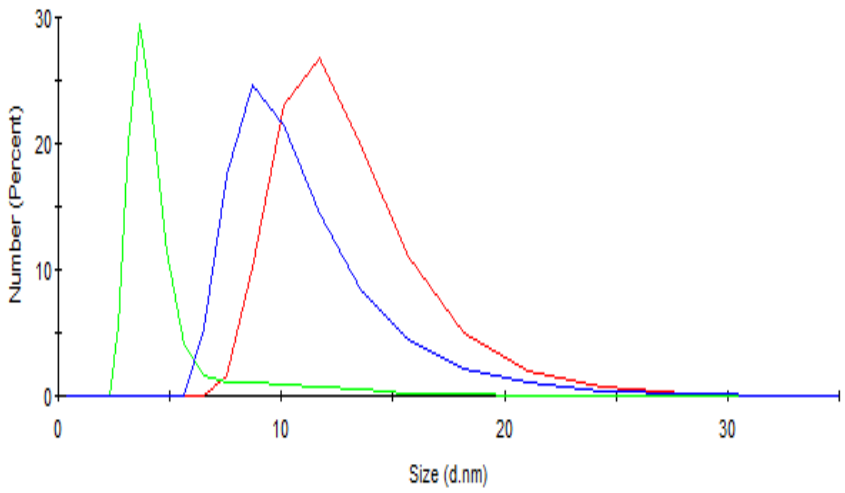

Figure 6: 4+ nanoparticles are about 10nm in size after ultrasonication
Similar methodology as that for Figure 5 was adopted. Size was measured by DLS after 5 minutes of ultrasonication. [Ce^{4+}] = 250µM.

The nanoparticle size did not change significantly with ultrasonication. This suggests that that there is no significant aggregation of nanoparticles over time. The average size seemed to peak at around 10nm which is well within the nano-world range of 1-100nm and thus will provide all the benefits of smaller size. A consistent size also ensures consistent activity for each batch of nanoparticles.

UV-Visible Spectra of Nanoparticles

Figure 7 shows the UV-Visible spectra of cerium oxide nanoparticles. Table 3 shows the resultant maxima and minima for different batches of nanoparticles used.

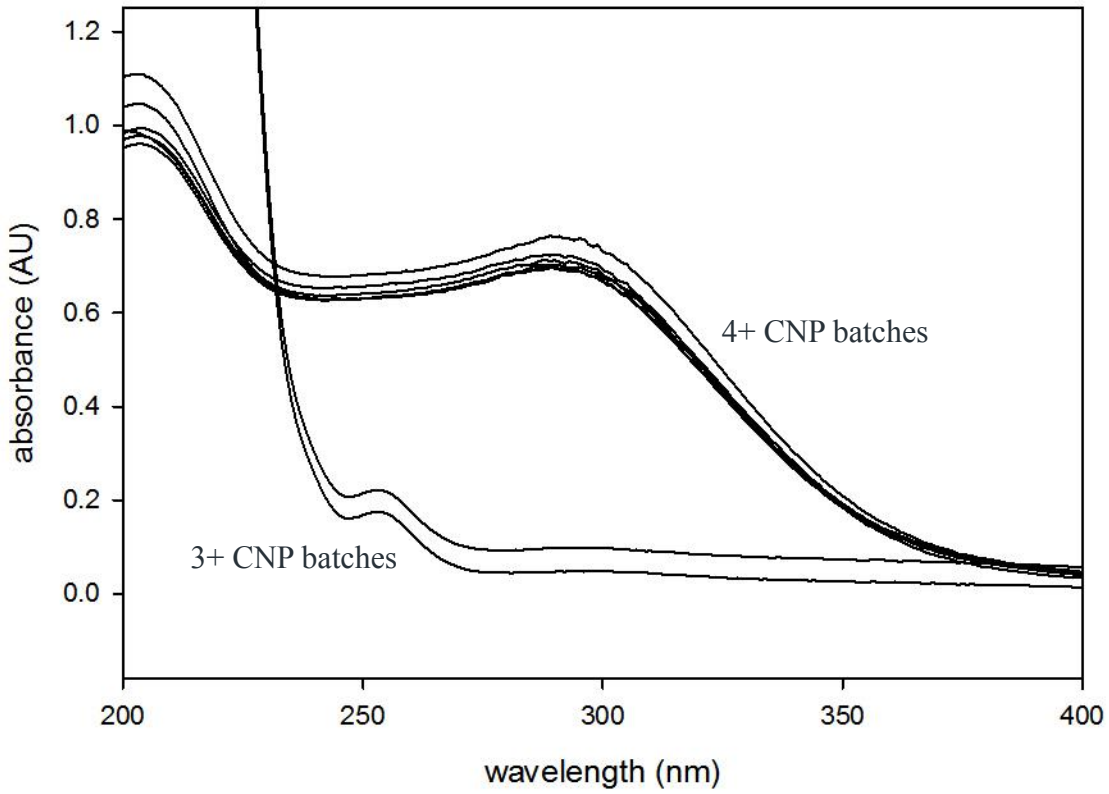

Figure 7: Different batches of cerium oxide nanoparticles have consistent UV-Visible spectra
UV-Visible spectra for different batches of 4+ and 3+ nanoparticles (both at 125µM) are shown from 200-400nm.

Several batches of cerium oxide nanoparticles had largely consistent spectra. This was an important result because it confirmed that all the experiments conducted in this project used fairly uniform batches of cerium oxide nanoparticles. The spectra of 4+ nanoparticles had a maximum at around 290nm and a minimum at around 242nm. The spectra for 3+ nanoparticles on the other hand had two maxima at around 253nm and 298nm and two minima at around 281nm and 247nm. The consistency in the absorbance of different batches suggests that their

concentrations were also fairly uniform. This suggests that 5mM of cerium in the solutions of nanoparticles led to a consistent nanoparticle concentration for all batches.

Table 3: Consistent maxima and minima for different batches of cerium oxide nanoparticles

Batch	Maxima(nm)	Absorbance(AU)	Minima(nm)	Absorbance(AU)
4+(6/18/13)	290.0	0.72511	242.0	0.65304
4+(12/19/13)	288.0	0.69664	242.0	0.62575
4+(4/2/14)	288.0	0.70123	---	-----
4+ sonicated(6/18/13)	289.0	0.76484	242.0	0.67697
4+ sonicated(12/19/13)	288.0	0.71349	242.0	0.63717
4+ sonicated(4/2/14)	289.0	0.69630	245.0	0.62834
3+	253.0 298.0	0.17581 0.04949	281.0 247.0	0.04508 0.16007
3+ sonicated	253.0 296.0	0.22240 0.09935	281.0 247.0	0.09337 0.20712

Dates on which 4+ nanoparticle samples were received are mentioned in brackets.

Role of Water in Phosphatase Activity

The role of water in the cleavage of phosphate from donors for the phosphatase activity of 4+ cerium oxide nanoparticles was demonstrated. Figure 8 shows the increase in rate of the reaction with the addition of water instead of methanol in the pNPP Assay.

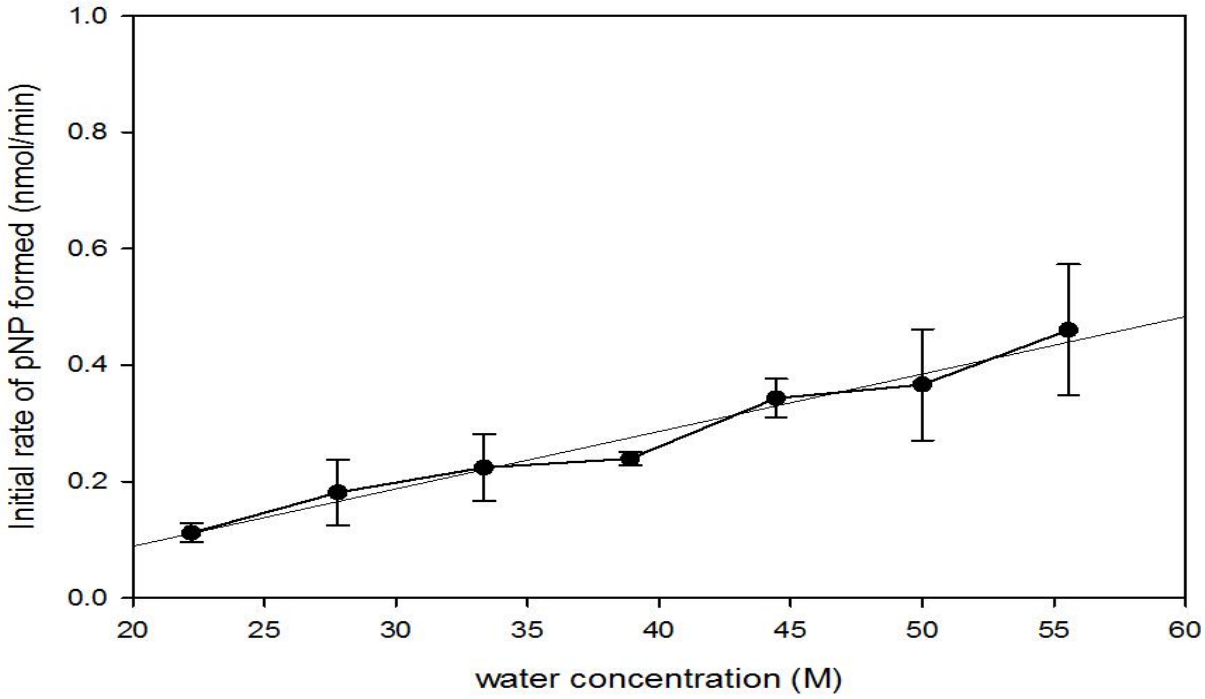

Figure 8: Phosphatase mimetic activity increases with addition of water in the pNPP assay Water was replaced by methanol in steps of 10% of the reaction volume (20-120µl). The actual concentration of water (M) in the reaction was calculated by using percentages of 55.55M and working backwards serially. [pNPP] =1.2mM and [Ce^{4+}] = 200µM.

The figure clearly shows that the phosphatase mimetic activity increases linearly with the addition of water to the reaction volume. This strongly suggests that the phosphatase activity is due to the hydrolytic cleavage of the phosphate group from the donor substrate. Figure 9 shows a similar result in the MUP assay. This time the rate is left in terms of Δintensity/min. The sudden spike at the last point can be attributed to the fact that the Em_{max} of the samples with methanol will be slightly different from the sample with no methanol (or only water). The curve is linear for the region that has methanol and this corroborates the results from the pNPP assay.

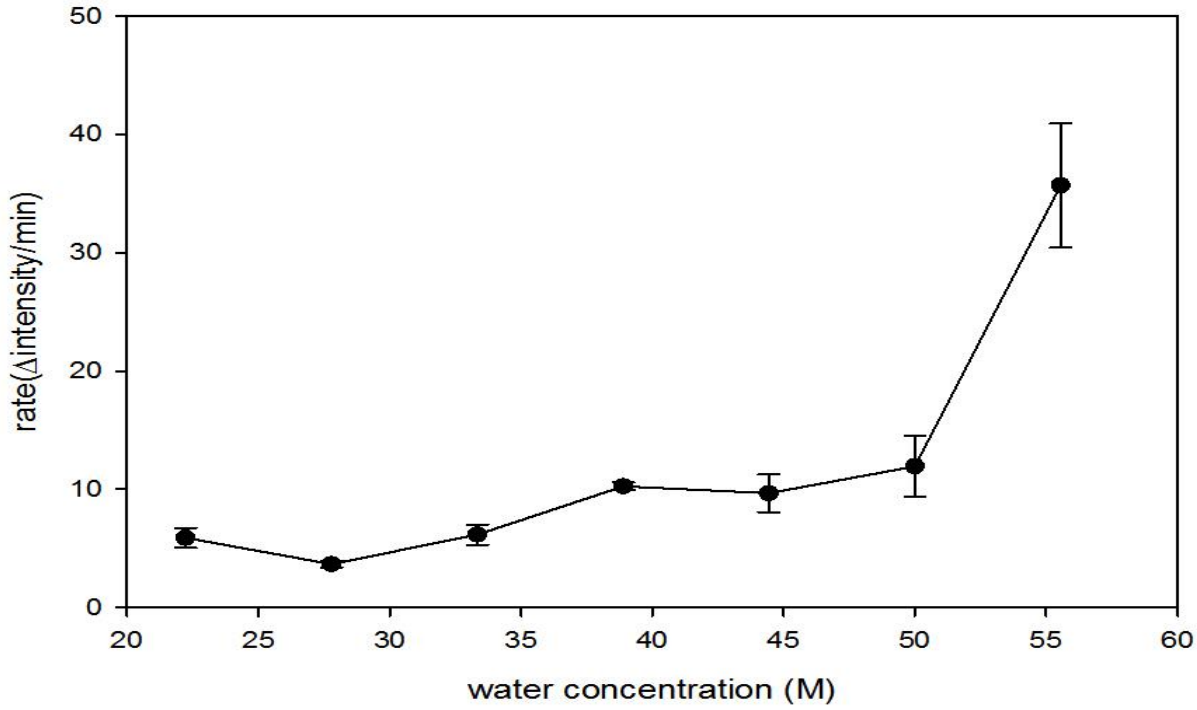

Figure 9: Phosphatase mimetic activity increases with addition of water in the MUP assay Similar methodology to that of Figure 8 was adopted. [MUP] =500µM and [Ce^{4+}] = 200µM.

To summarize, the results clearly point at hydrolytic chemistry being involved in the cleavage of phosphate from donor substrates. The adsorption of water on the surface of 4+ cerium oxide nanoparticles makes them more active for phosphatase mimetic activity.

Mechanism of Phosphatase Activity

The results for the experiments conducted to confirm phosphatase activity of cerium oxide nanoparticles are discussed below. Figure 10 shows the phosphatase activity of different catalysts in the pNPP assay. As can be seen from the figure water based 4+ cerium oxide nanoparticles exhibit the highest level of phosphatase activity. HMT-ceria showed some activity and this is useful when considered with the fact that HMT-ceria has a better uptake by cells than

water based cerium oxide nanoparticles [5]. All other catalysts, including doped forms of cerium oxide showed close to no phosphatase activity.

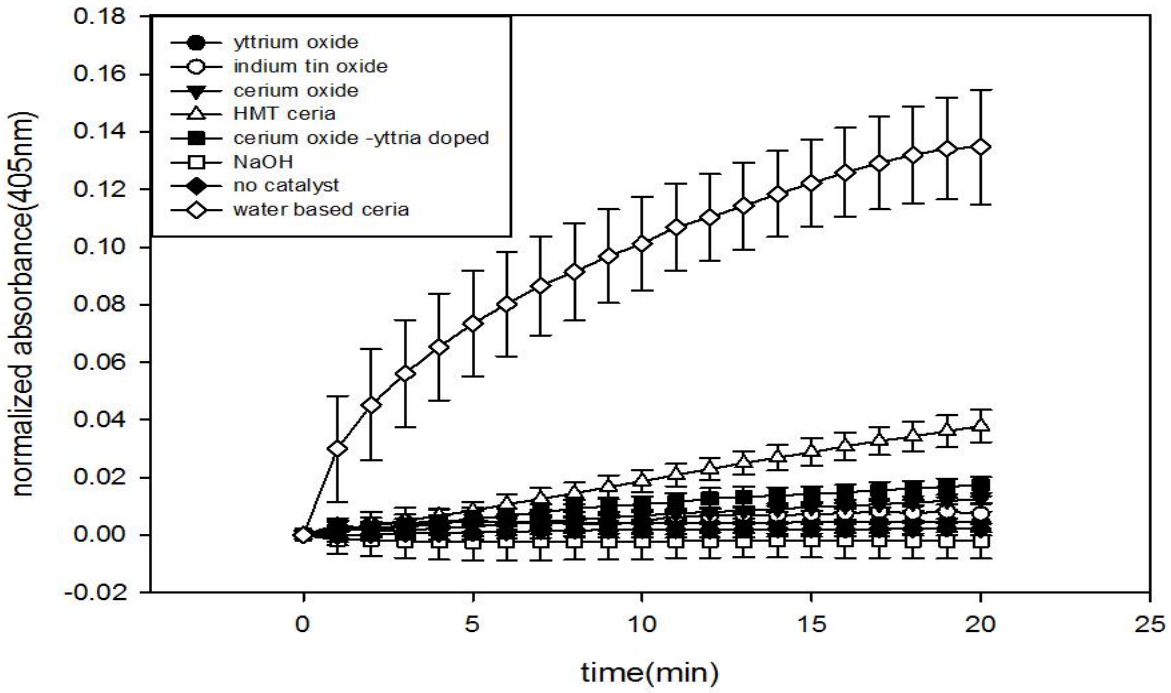

Figure 10: Water based nanoceria exhibits higher phosphatase activity than other forms of ceria Various metal oxides and doped forms of ceria were tested for phosphatase activity. [pNPP] = 1.2mM and [Ce^{4+}] = 100µM.

Figure 11 shows a comparison between the phosphatase activities of 4+ and 3+ cerium oxide nanoparticles in the pNPP assay. Clearly the 4+ cerium oxide nanoparticles possess phosphatase activity while the 3+ cerium oxide nanoparticles do not. The minimal activity shown by 3+ nanoparticles saturates within minutes.

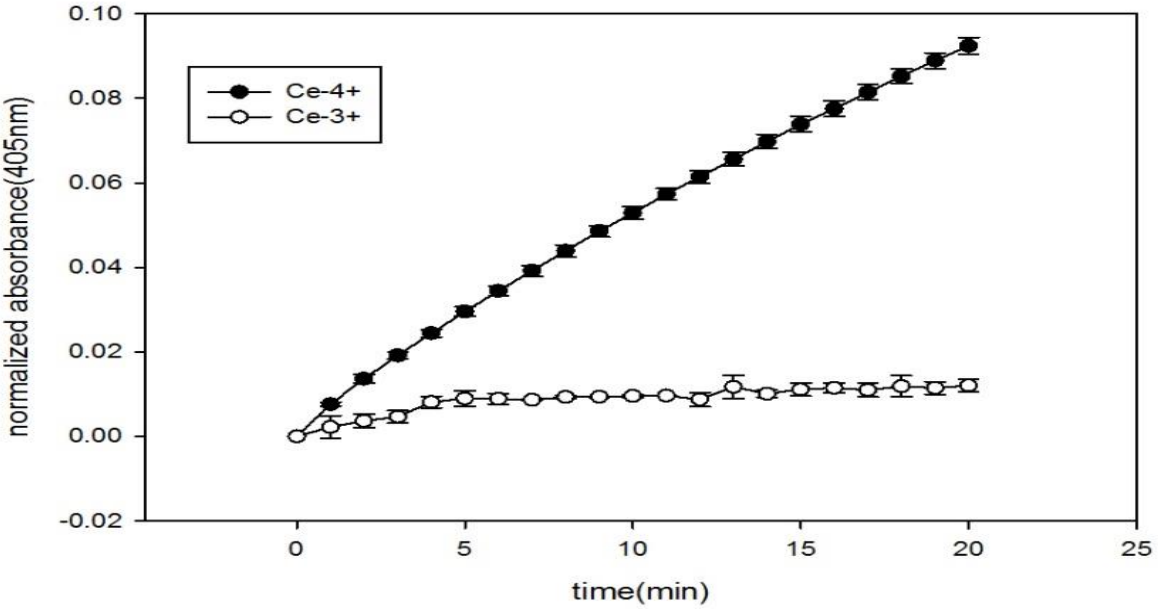

Figure 11: 4+ nanoparticles exhibit phosphatase mimetic activity while 3+ nanoparticles do not Similar methodology to that of Figure 10 was adopted. [pNPP] = 1.2mM and [Ce^{4+}] = 100µM.

Figure 12 shows the saturation of phosphatase activity of 4+ nanoparticles in the pNPP assay. The figure clearly shows that rate of reaction remains almost linear over long periods of time. At the end of 60 minutes the absorbance curve for 1.2mM pNPP begins flattening but the 9.6mM curve remains on its increasing course. This result illustrates that cerium oxide nanoparticles can remain phosphatases over large periods of time given that there is enough substrate to carry the reaction forward.

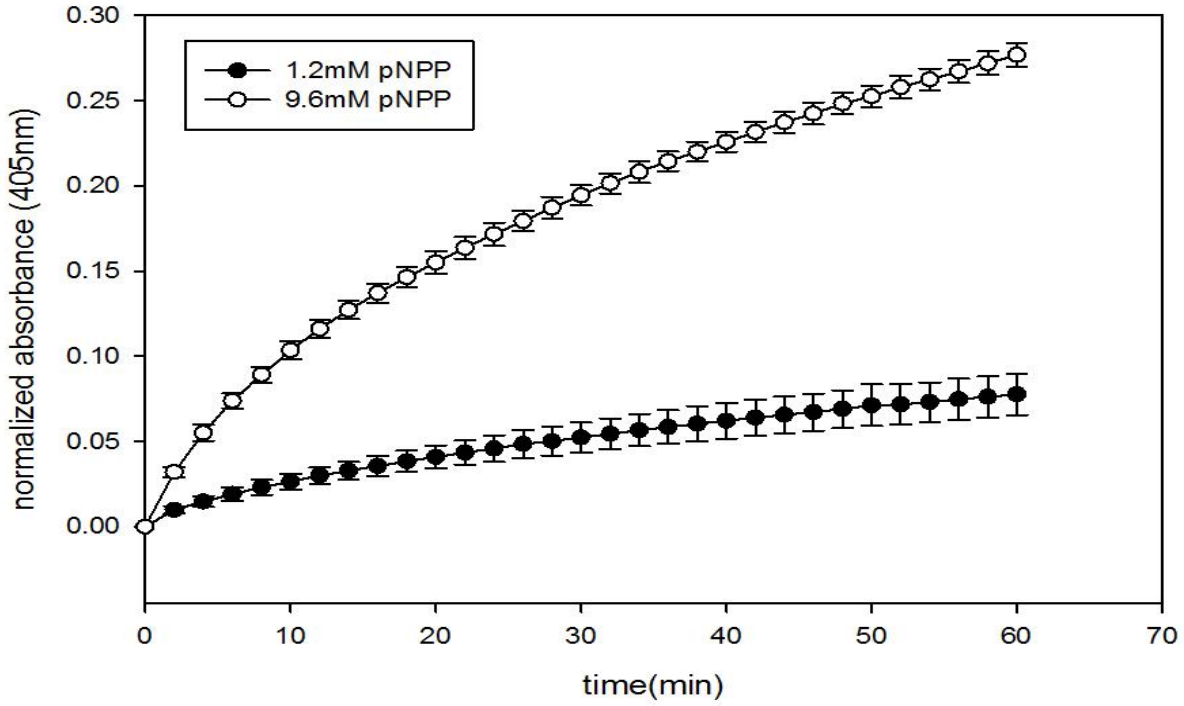

Figure 12: Phosphatase activity of nanoceria stays linear over long periods of time
Similar methodology to that of Figure 10 was adopted. [pNPP] = 1.2mM and 9.6mM and [Ce^{4+}] = 200µM. The activity just begins to saturate at 60 minutes for the lower concentration of pNPP.

Figure 13 shows a sudden spike in phosphatase activity after replenishing substrate (1.2mM pNPP) at the end of 60 minutes. The figure clearly shows that the phosphatase activity was saturated at the end of 60 minutes and spiked again with the addition of fresh substrate. This strengthens the claim that the 4+ nanoparticles remain as such at the end of the reaction and can be reused as phosphatases.

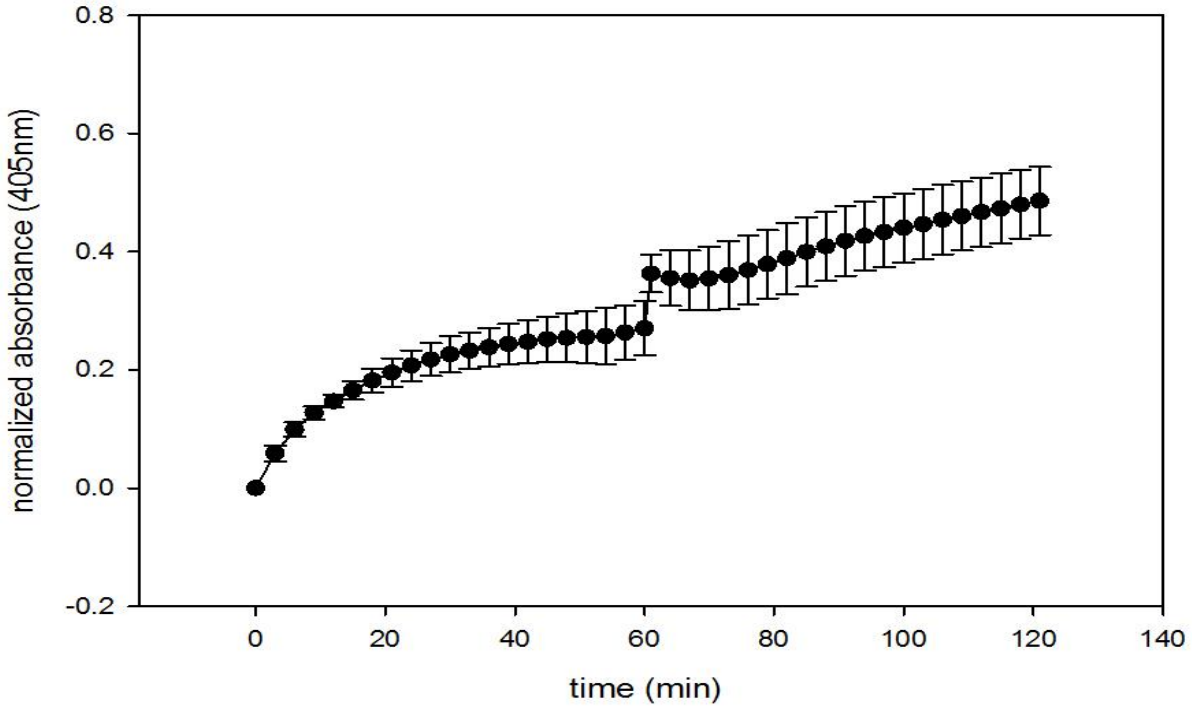

Figure 13: Phosphatase activity is revived after replenishment of substrate
Similar methodology to that of Figure 12 was adopted. [pNPP] = 1.2mM and [Ce^{4+}] = 200µM. Reaction mix was replenished with 1.2mM pNPP at the end of 60 minutes. This caused a revival of phosphatase activity.

Figure 14 shows the Michaelis-Menten curve for kinetics of phosphatase activity in the pNPP assay without any inhibitors. The V_{max} and K_m values were 0.4371nmol/min and 0.7373mM respectively.

The figure clearly shows that cerium oxide nanoparticles follow a Michaelis-Menten profile for phosphatase activity. The Y axis is reported as the initial rate of pNP formed and is equal to the rate of phosphate formed.

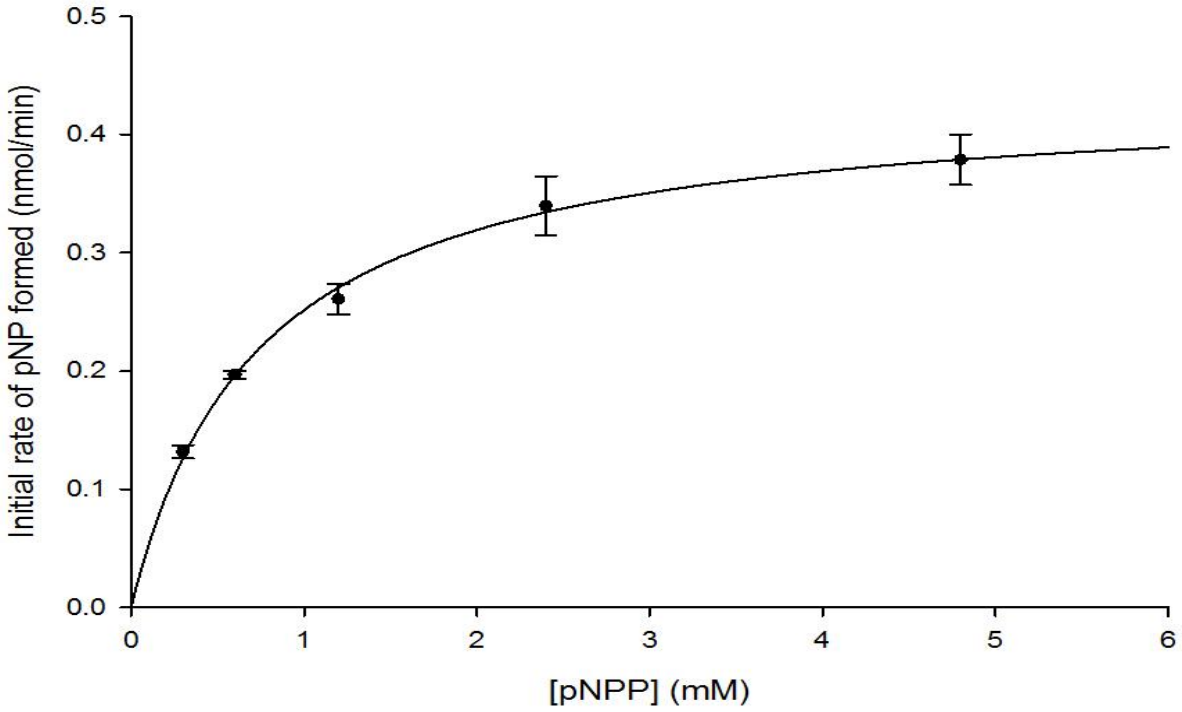

Figure 14: Phosphatase activity of 4+ nanoparticles follows Michaelis-Menten kinetics Different concentrations of pNPP were used – 0.3, 0.6, 1.2, 2.4, and 4.8mM. $[Ce^{4+}]$ = 200µM. The initial rate of the reaction was calculated by using the change in absorbance (Δabs/min) and the molar extinction coefficient for pNPP ($18.5mM^{-1}cm^{-1}$).

Figure 15 shows the Lineweaver-Burk plot for the same experiment. The reciprocal data seems to fit well linearly and strengthens the claim that cerium oxide nanoparticles follow the Michaelis-Menten model for enzyme kinetics.

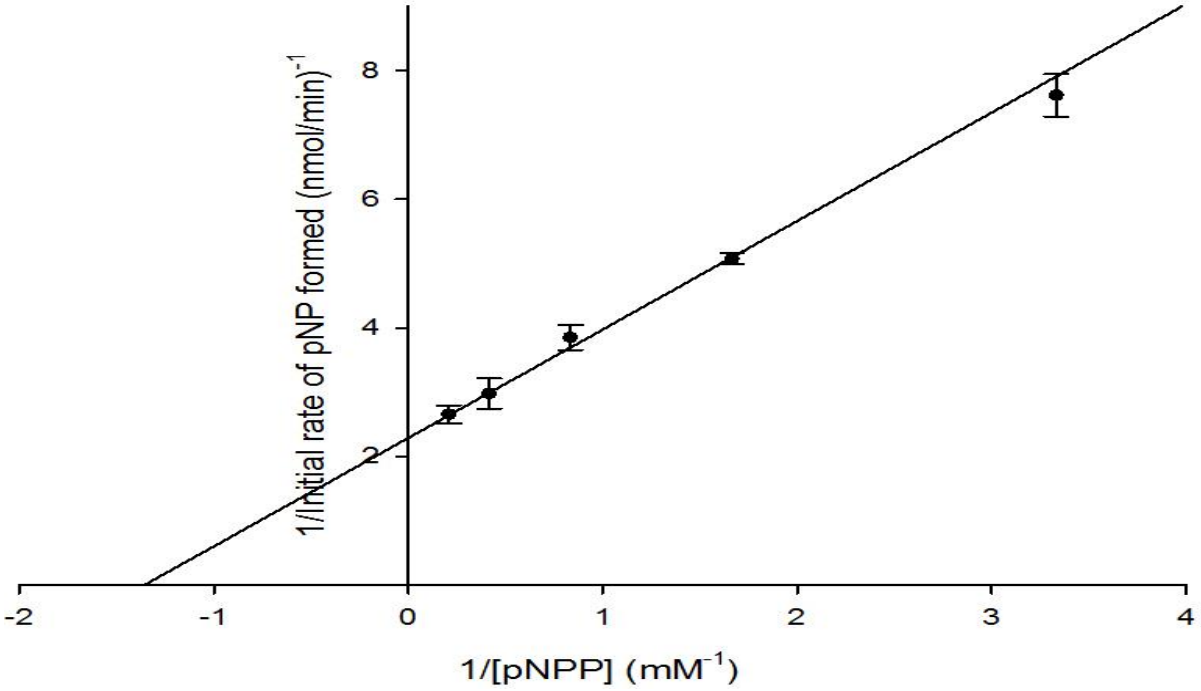

Figure 15: Phosphatase activity follows Michaelis-Menten kinetics - Lineweaver-Burk plot
Similar methodology as that for Figure 14 was adopted.

Figure 16 shows a comparison of the phosphatase activity of 4+ and 3+ nanoparticles using the MUP assay which measures fluorescence. The figure clearly corroborates the data from the pNPP assay. The 3+ cerium oxide nanoparticles again have close to no activity. The MUP assay is a more sensitive assay than the pNPP assay and thus reiterates that 3+ nanoparticles are not catalysts when compared to 4+ nanoparticles. Figure 17 shows the result for an experiment to saturate the phosphatase activity in the MUP assay. The figure clearly shows that even after 2 hours the rate of increase in intensity is linear for 4+ nanoparticles. This shows that cerium oxide nanoparticles can sustain their phosphatase activity over long periods of time.

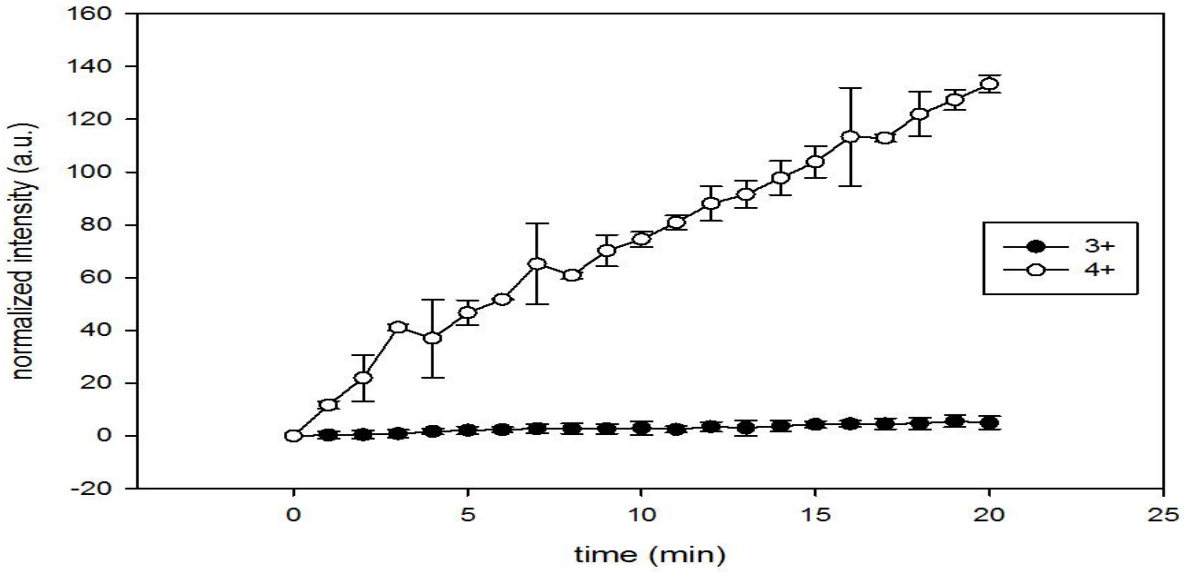

Figure 16: 4+ nanoparticles exhibit phosphatase mimetic activity in the MUP assay
MUP was excited at 360nm.and the change in intensity of fluorescence was measured at 449nm. [MUP] = 500µM and [Ce^{4+}] = 200µM.

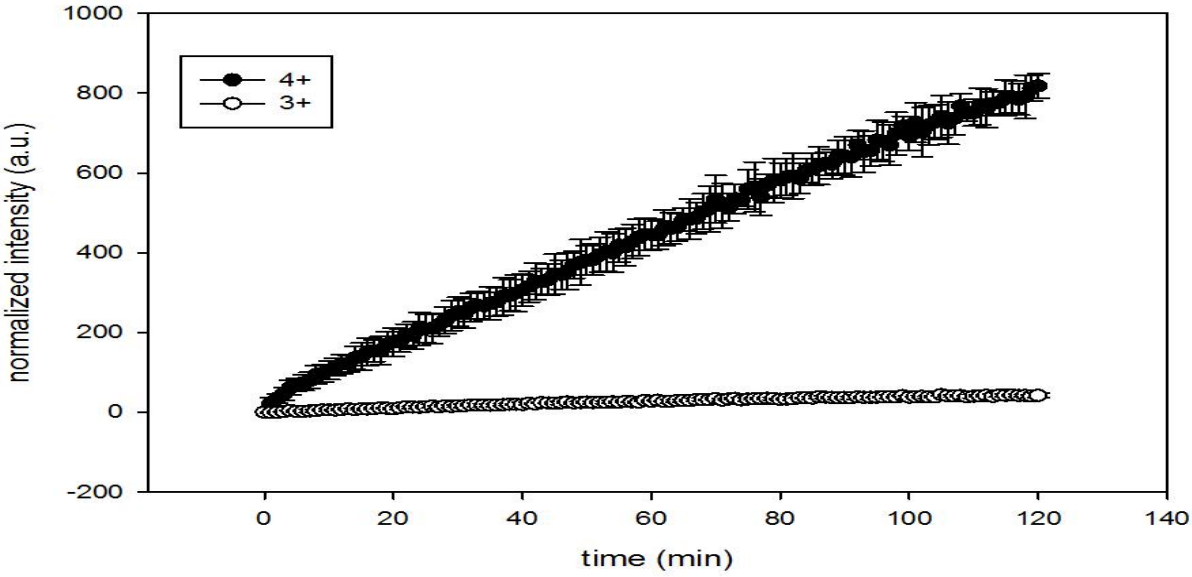

Figure 17: Phosphatase activity of 4+ nanoparticles remains linear over long periods of time (MUP assay)
Similar methodology as that of Figure 16 was adopted. [MUP] = 1mM and [Ce^{4+}] = 200µM.

Figure 18 shows the result for an experiment conducted using the EnzChek® Assay on ATP. This graph was generated after calculating the phosphate in nmol/well from the standard curve. This result confirms that cerium oxide nanoparticles can act as phosphatases for bio-relevant substrates as well. Curve 1, 2 and 3 indicate the triplicates used in the experiment.

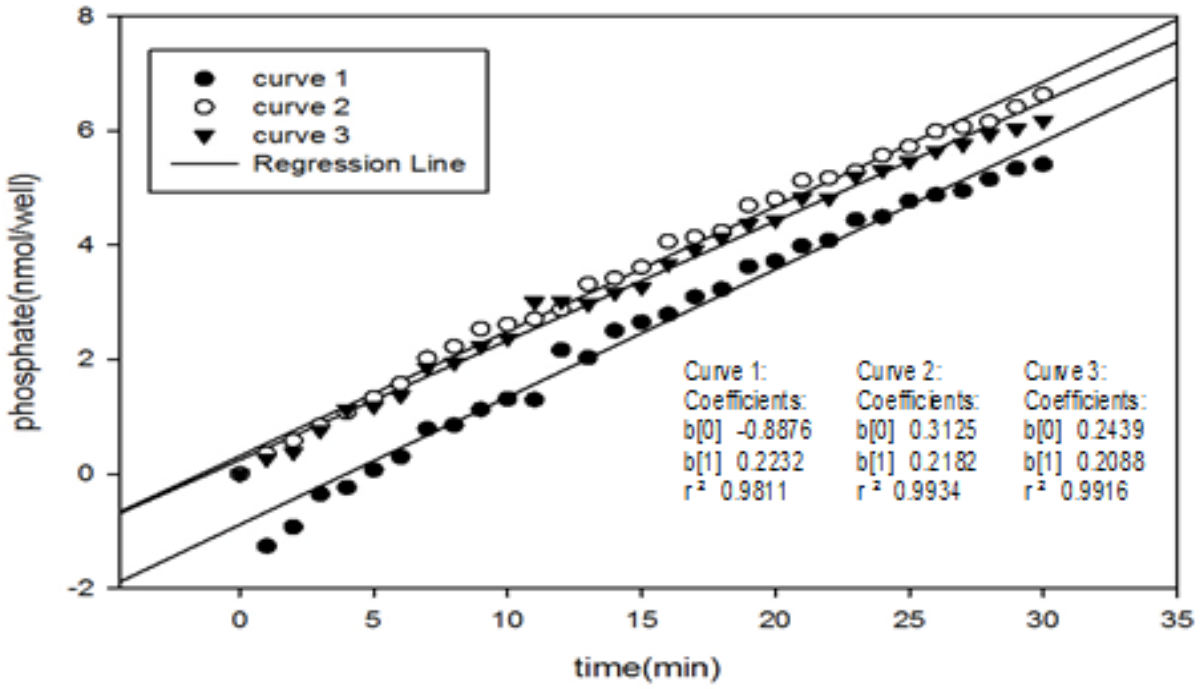

Figure 18: 4+ nanoparticles exhibit phosphatase activity on ATP (EnzChek® assay)
The enzymatic conversion of MESG by purine nucleoside phosphorylase into ribose 1-phosphate and 2-amino-6-mercapto-7-methylpurine was followed at 360nm. [ATP] = 100µM and [Ce^{4+}] = 200µM. Phosphate standard was used to calculate the nmol of phosphate/well.

The Malachite Green assay results were not satisfactory as we had to simulate kinetic reactions by adding ATP at different points and then calculate the initial rate. The time points between readings could not be maintained precisely since the assay involved the addition of stopping

reagents (A and B). Even though a concurrent trend was noticed, the error in the data points was too large. The EnzChek® assay provided data for ATP as a substrate.

In summary, phosphatase activity was shown by pNPP, MUP, MG and EnzChek® assays. It was modeled to a Michaelis-Menten profile in the pNPP assay indicating that it follows saturation based kinetics.

Inhibition of Phosphatase Activity

Three anions were identified that inhibited the phosphatase mimetic activity in a dose dependent manner – tungstate, molybdate and arsenate. Sulfate and selenate did not show significant inhibition of phosphatase activity. Figure 19 shows the Michaelis-Menten curve for the dose dependent inhibition of phosphatase activity using tungstate.

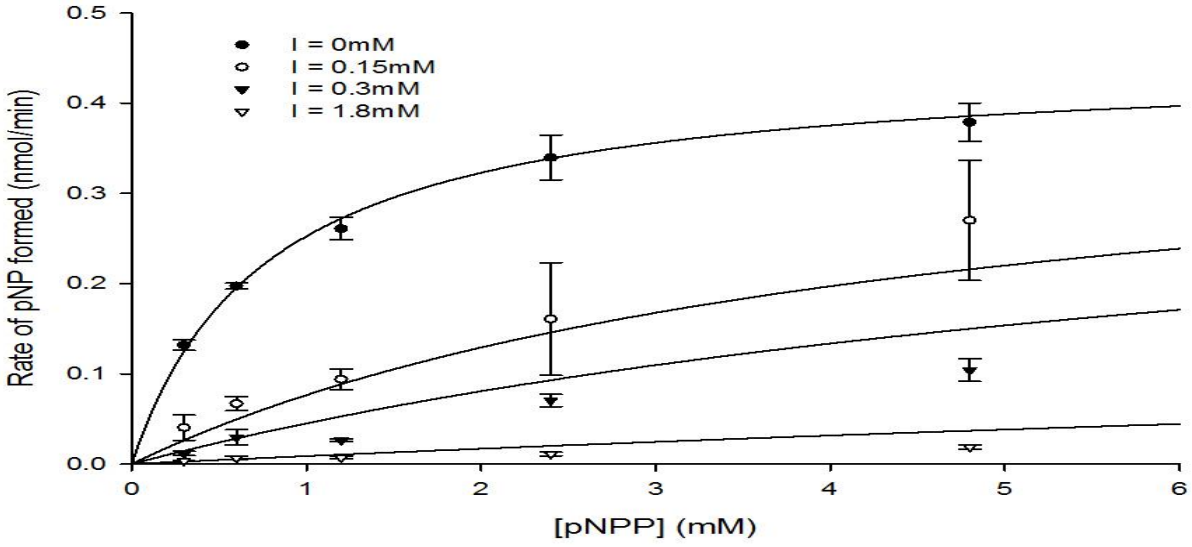

Figure 19: Tungstate is a potent inhibitor of phosphatase activity - Michaelis-Menten curve
Kinetic studies were performed over [pNPP] = 0.3, 0.6, 1.2, 2.4 and 4.8mM and [tungstate] = 0, 0.15, 0.3 and 1.8mM. Rates were calculated in nmol/min using molar extinction coefficient for pNPP ($18.5 mM^{-1}cm^{-1}$). Partial mixed inhibition was chosen as a suitable model for inhibition.

The figure shows a clear drop in activity as tungstate concentration (in mM) increases. At a high concentration of 1.8mM the activity is nearly undetectable. Figure 20 shows the Lineweaver-Burk plot for the same experiment. The data for 1.8mM of inhibitor does not fit well with the trend line. This is an inherent characteristic of double reciprocal plots as the errors are magnified when they are inverted. Also, the actual nmol/min of phosphate being formed at 1.8mM of tungstate was extremely close to zero. Being so close to the detection limit explains the rather large error bars.

A partial mixed inhibition model was chosen to explain tungstate inhibition. The kinetic parameters were as follows:-

V_{max} = 0.45nmol/min, K_m = 0.77mM, K_i = 0.03mM, α = 66.14, β = 1.02 x 10^{-4}.

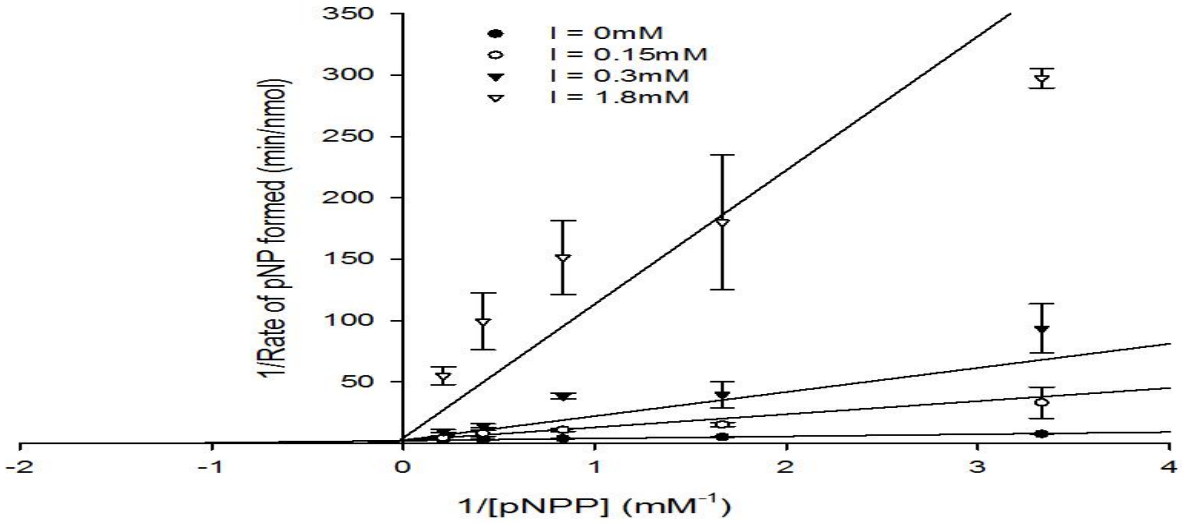

Figure 20: Tungstate is a potent inhibitor of phosphatase activity - Lineweaver-Burk plot
Similar methodology as that for Figure 19 was adopted.

Figure 21 shows the Michaelis-Menten curve for the dose dependent inhibition of phosphatase activity using molybdate. Figure 22 shows the Lineweaver-Burk plot for the same experiment. A similar explanation can be provided for these figures. A partial mixed inhibition model was chosen to explain molybdate inhibition. The kinetic parameters were as follows:-

V_{max} = 0.48nmol/min, K_m = 1.02mM, K_i = 0.10mM, α = 4.08, β = 1.17 x 10^{-2}.

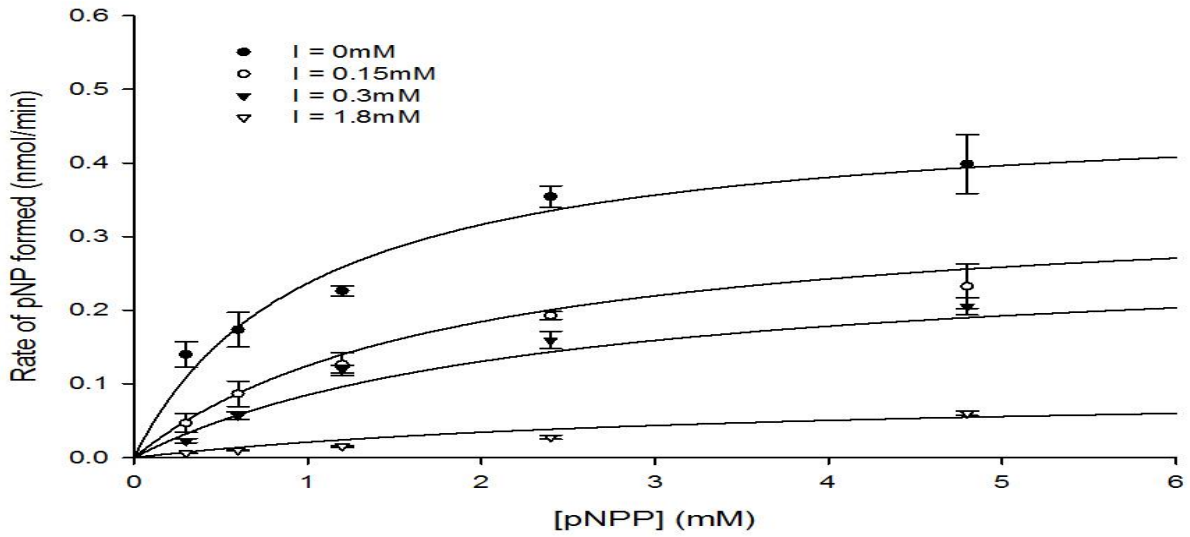

Figure 21: Molybdate is a potent inhibitor of phosphatase activity - Michaelis-Menten curve
Kinetic studies were performed over [pNPP] = 0.3, 0.6, 1.2, 2.4 and 4.8mM and [molybdate] = 0, 0.15, 0.3 and 1.8mM. Rates were calculated in nmol/min using molar extinction coefficient for pNPP ($18.5mM^{-1}cm^{-1}$). Partial mixed inhibition was chosen as a suitable model for inhibition.

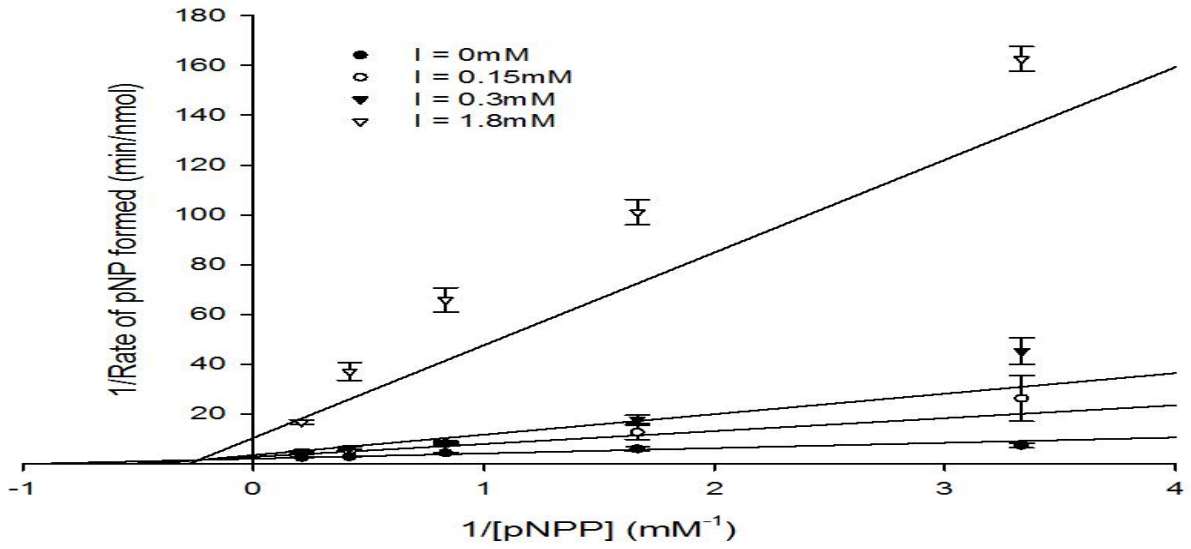

Figure 22: Molybdate is a potent inhibitor of phosphatase activity - Lineweaver-Burk plot
Similar methodology as that for Figure 21 was followed.

Figure 23 shows the Michaelis-Menten curve for the dose dependent inhibition of phosphatase activity using arsenate. Figure 24 shows the Lineweaver-Burk plot for the same experiment. A similar explanation can be provided for these figures. A partial mixed inhibition model was chosen to explain arsenate inhibition. The kinetic parameters were as follows:-

V_{max} = 0.45nmol/min, K_m = 0.76mM, K_i = 0.04mM, $\alpha = 6.25 \times 10^5$, $\beta = 0.55$.

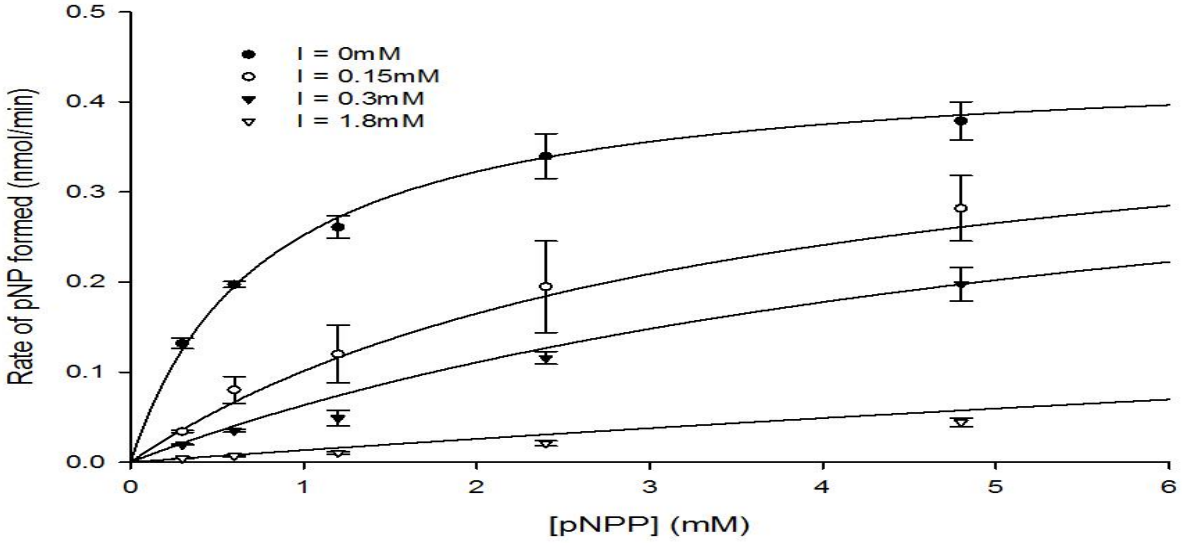

Figure 23: Arsenate is a potent inhibitor of phosphatase activity - Michaelis-Menten curve
Kinetic studies were performed over [pNPP] = 0.3, 0.6, 1.2, 2.4 and 4.8mM and [arsenate] = 0, 0.15, 0.3 and 1.8mM. Rates were calculated in nmol/min using molar extinction coefficient for pNPP ($18.5mM^{-1}cm^{-1}$). Partial mixed inhibition was chosen as a suitable model for inhibition.

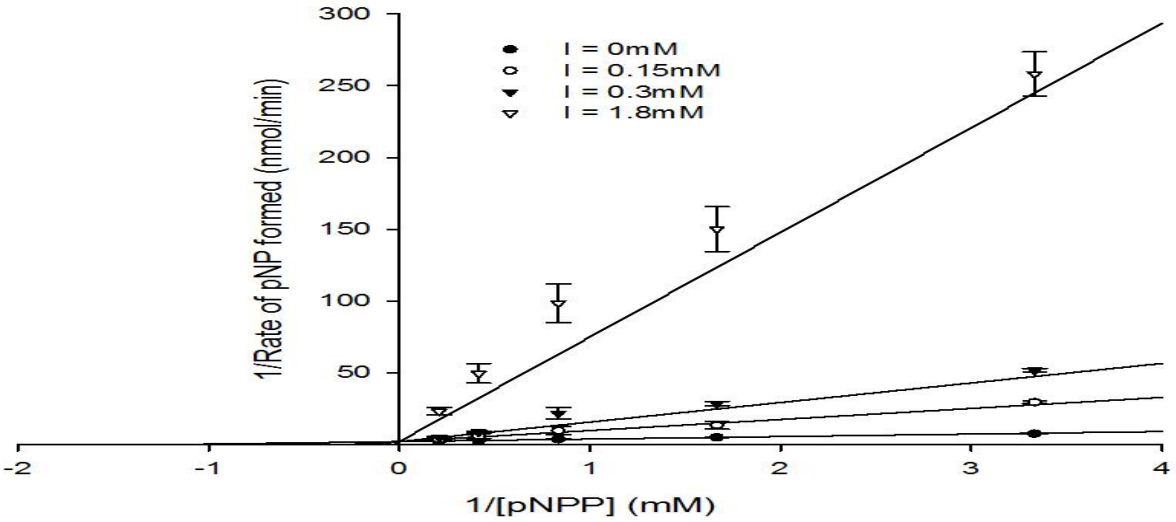

Figure 24: Arsenate is a potent inhibitor of phosphatase activity - Lineweaver-Burk plot
Similar methodology as that for Figure 23 was adopted.

Inhibitory anions appear to block the active sites of the nanoparticles. Nanoparticle-Inhibitor-Substrate complexes may have formed on the surface of the nanoparticles and led to slowing down of the reaction. An analog for this would be the EIS complex formed in enzyme inhibition. α values predict type of inhibition to be mixed while a non-zero value for β suggests that the inhibition is not full. Some product effectively leaks out through the conversion of EIS to E, I and P. This is an important consideration when trying to inhibit the activity of an enzymatic system. Here a distinction can be made for the β values of arsenate vs those for tungstate and molybdate. It is clear that tungstate and molybdate follow almost full inhibition while arsenate inhibition is quite weak in the sense that about 33% of the product is formed from the EIS complex. Table 4 summarizes the inhibition (parameters and nature) for all three anions.

Table 4: Inhibition of phosphatase activity by anions

Parameter	Tungstate	Molybdate	Arsenate
V_{max} (nmol/min)	0.45	0.48	0.45
K_m (mM)	0.77	1.02	0.76
K_i (mM)	0.03	0.10	0.04
A	66.14	4.08	6.25e+5
B	1.02e-4	1.17e-2	0.55
Type of inhibition	$\alpha >> 1$ Mixed inhibition	α close to 1 Mixed inhibition (Close to being Non-Competitive)	$\alpha >>> 1$ Mixed inhibition
Degree of inhibition	$\beta \rightarrow 0$ Follows partial inhibition to a small extent	$\beta \rightarrow 0$ Follows partial inhibition to a small extent	$\beta > 0$ Follows partial inhibition to a large extent

Sulfate and selenate did not show significant inhibition of the activity. Figure 25 shows the graph for change in absorbance at 405nm with addition of sulfate. Even after addition of 1mM of sulfate, there was no significant drop in the rate of the reaction. This suggests that sulfate has a chemistry which does not support the formation of Nanoparticle-Inhibitor-Substrate complex and thus it cannot inhibit the phosphatase activity. Figure 26 shows a similar graph for selenate. A similar inference can be drawn for selenate.

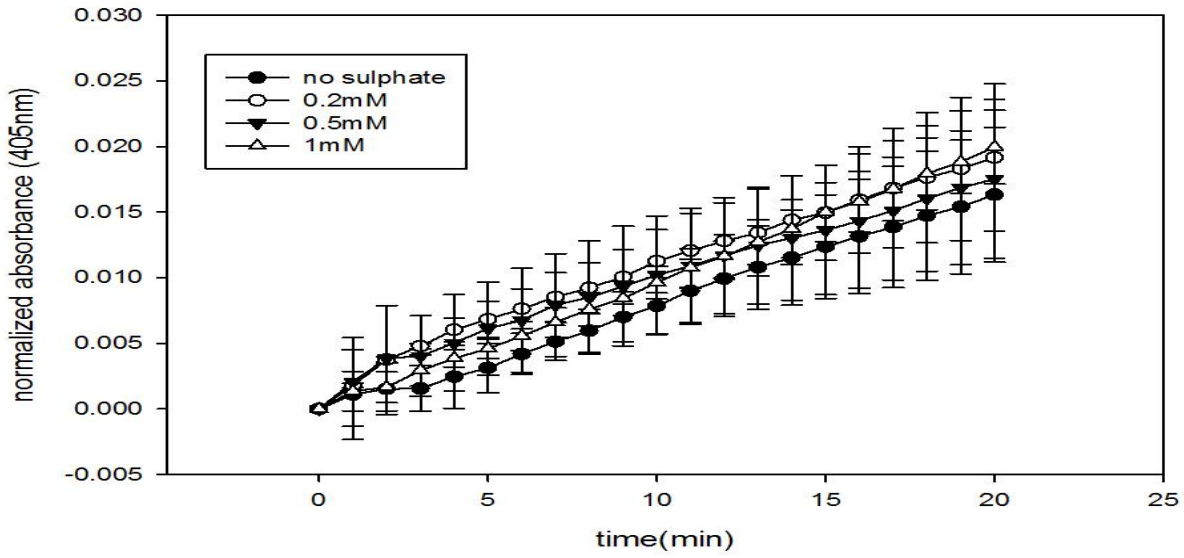

Figure 25: Sulfate does not inhibit phosphatase activity
Dose dependent inhibition of phosphatase activity was not observed by using [sulfate] = 0, 0.2, 0.5 and 1mM. [pNPP] = 1.2mM and [Ce^{4+}] = 200µM.

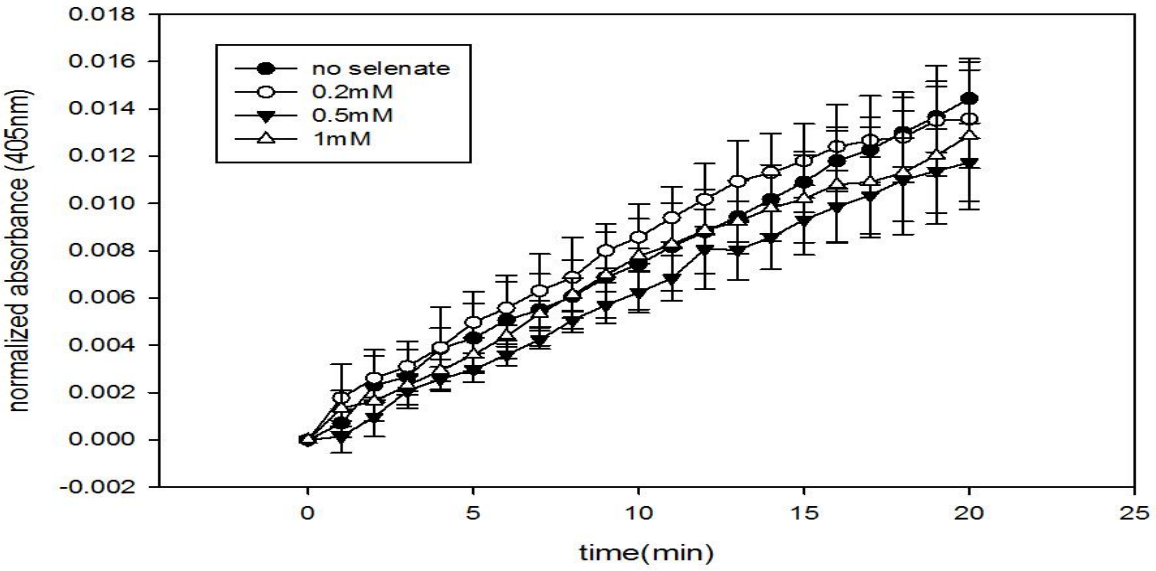

Figure 26: Selenate does not inhibit phosphatase activity
Dose dependent inhibition of phosphatase activity was not observed by using [selenate] = 0, 0.2, 0.5 and 1mM. [pNPP] = 1.2mM and [Ce^{4+}] = 200µM.

The MUP Assay was used to confirm the inhibition of phosphatase activity. There was a dose dependent decrease in intensity with increasing concentrations of arsenate (25, 50, 100 and 200µM).

The results for the Malachite Green assay were again unsatisfactory and hence EnzChek® assay results were used to confirm inhibition of phosphatase activity when ATP was the substrate. There was a decrease in phosphatase activity in the EnzChek® assay with addition of tungstate. The enzyme coupled reaction was found to be interfering results when arsenate was used.

To summarize, the results clearly indicate that anions can form complexes on the surface of nanoparticles and block their active sites. This explains why their addition leads to a reduction in

rate of the reaction. R^2 and AICc values for the models obtained were in favor of partial mixed inhibition but the degree of inhibition varied from anion to anion.

Phosphatase Activity of Biological Phosphatase

Calf Intestinal Phosphatase (Alkaline) was a superior phosphatase when compared to 4+ cerium oxide nanoparticles. CIP at a concentration of 570nM exhibited roughly the same change in absorbance as the cerium oxide nanoparticles that had a cerium concentration of 200µM. The actual concentration of the active sites of these nanoparticles was unknown. The phosphatase activity of CIP was also inhibited by tungstate, molybdate and arsenate.

The results confirm that cerium oxide nanoparticles are weak phosphatases when compared to biological phosphatases. Their phosphatase activity however, can be used as a model catalytic activity and can provide information on bioavailability and toxicity.

Oxidation State of Cerium Oxide Nanoparticles

The results from XPS data with and without inhibitors are shown below. The values for Binding Energy of electrons of cerium atoms are plotted against intensity of signal. Figures 27-30 show the results for XPS analysis on 4+ cerium oxide nanoparticles with and without inhibitors (tungstate, molybdate and arsenate). Figures 31-34 show the results for XPS analysis on 3+ cerium oxide nanoparticles with and without inhibitors (tungstate, molybdate and arsenate). The figures were compared to notice any obvious deviations in peaks. The 917nm peak (representing Ce^{4+}) decreased in area as the concentration of Ce^{3+} increased.

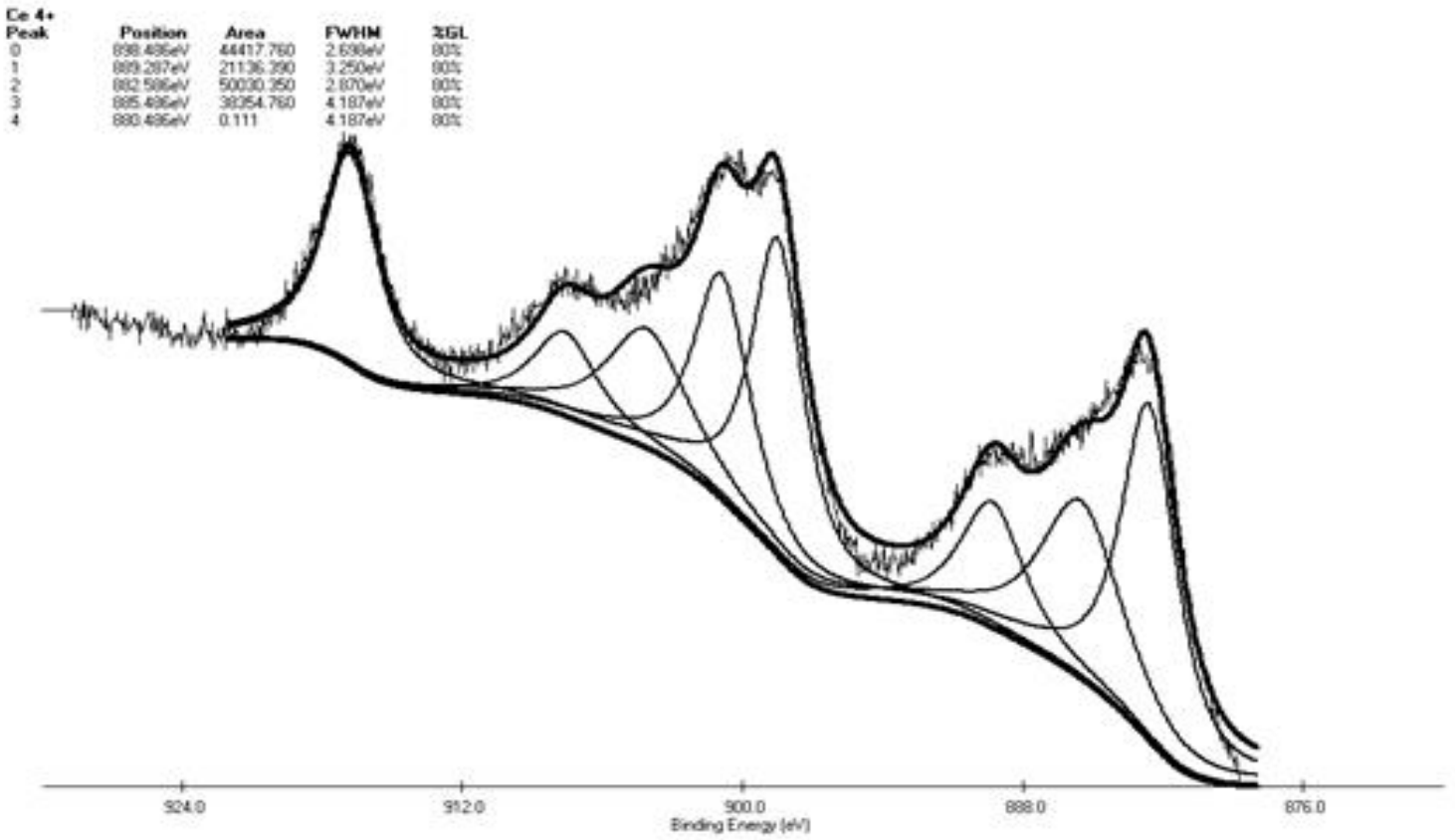

Figure 27: Binding energy spectrum for 3d orbital of Ce^{4+} nanoparticles

Nanoparticle solution with Ce^{4+} at 5mM was repeatedly applied to a silicon wafer and allowed to dry till a visible layer was noticeable. The binding energy spectrum for the 3d orbital of cerium was then generated using XPS.

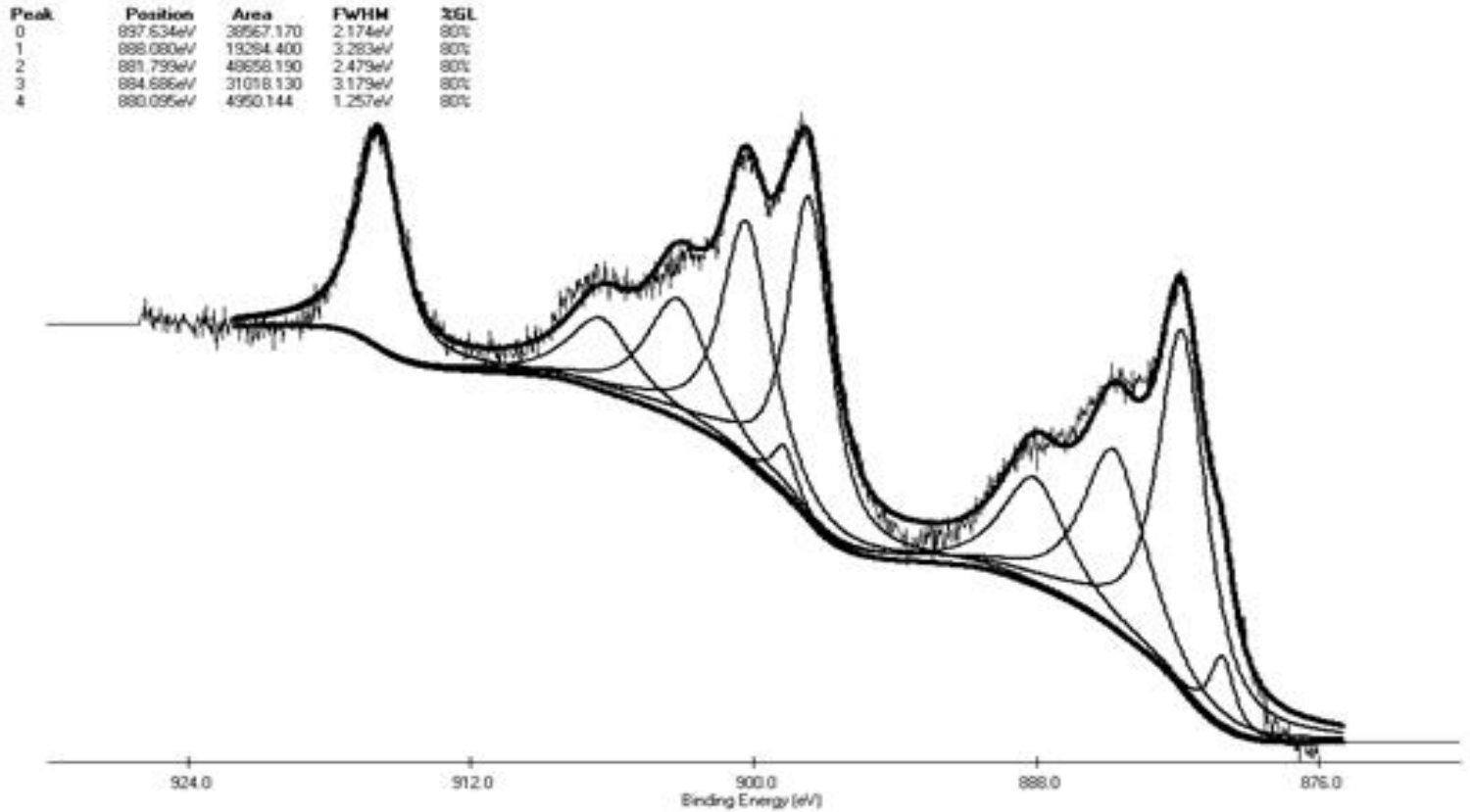

Figure 28: Tungstate does not significantly alter the binding energy spectrum for 4+ nanoparticles
Similar methodology as that for Figure 27 was adopted. Equimolar concentration of tungstate was mixed with nanoparticle solution and applied to a silicon wafer.

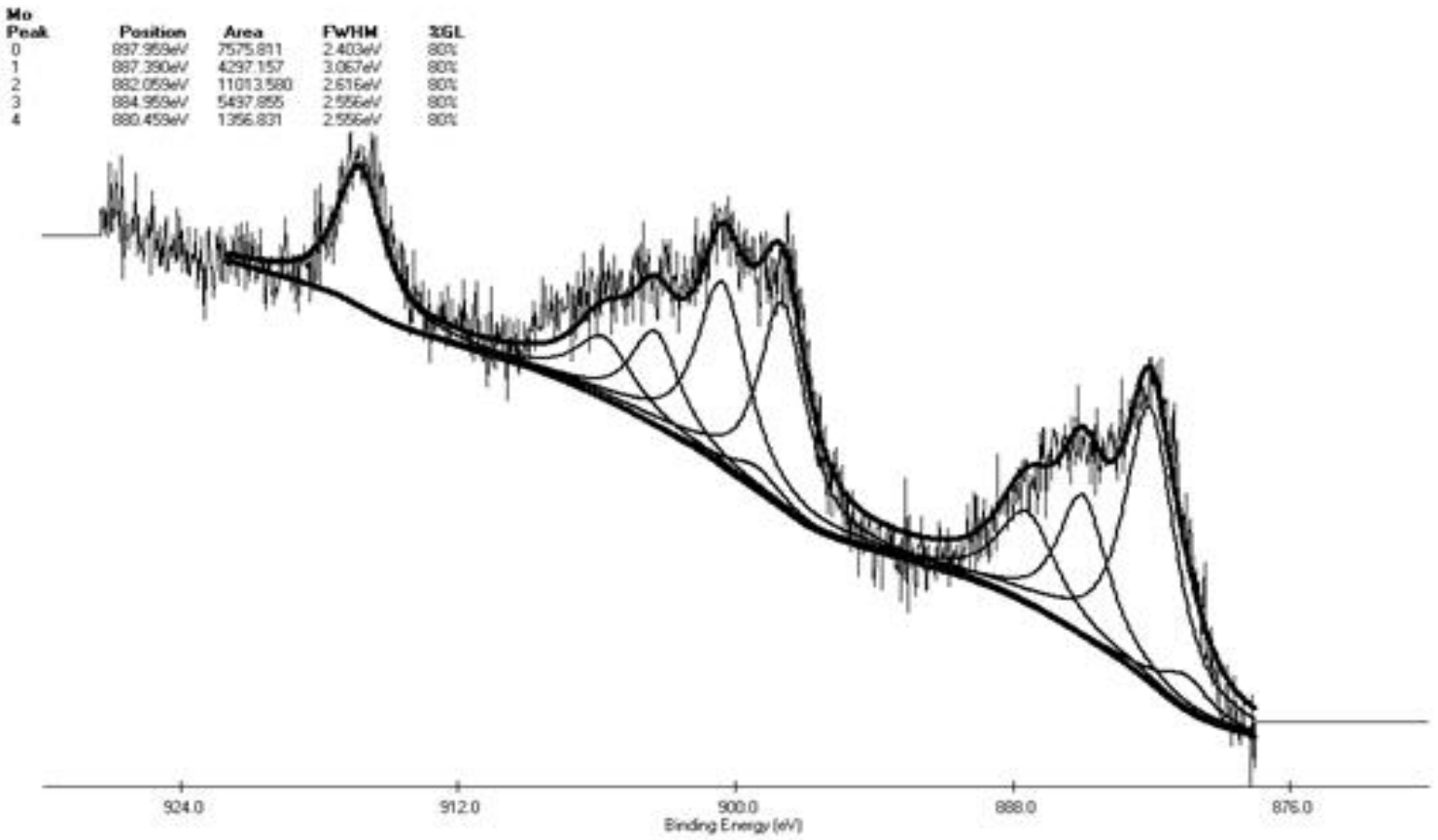

Figure 29: Molybdate does not significantly alter the binding energy spectrum for 4+ nanoparticles
Similar methodology as that for Figure 27 was adopted. Equimolar concentration of molybdate was mixed with nanoparticle solution and applied to a silicon wafer.

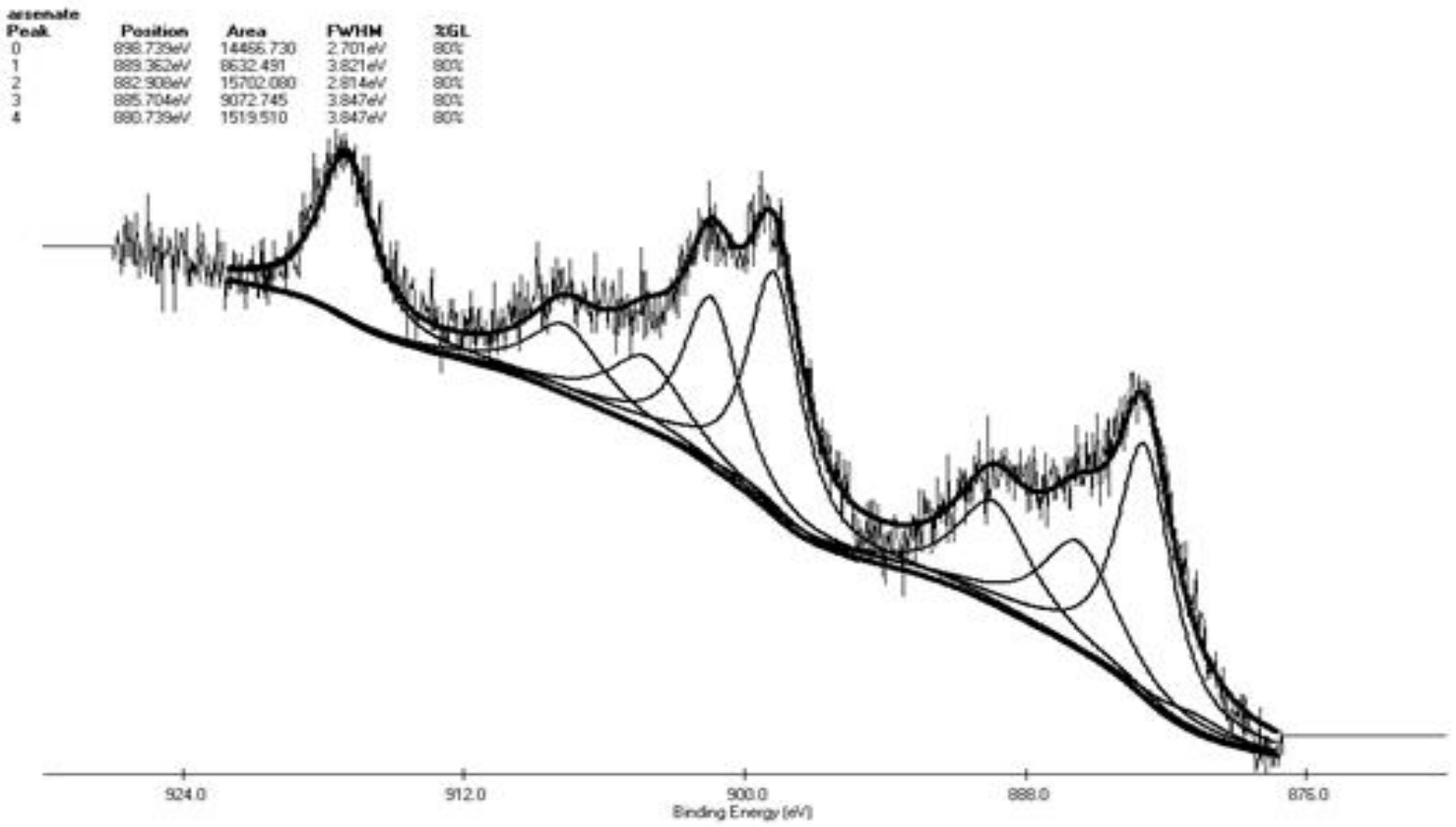

Figure 30: Arsenate significantly alters the binding energy spectrum for 4+ nanoparticles
Similar methodology as that for Figure 27 was adopted. Equimolar concentration of arsenate was mixed with nanoparticle solution and applied to a silicon wafer.

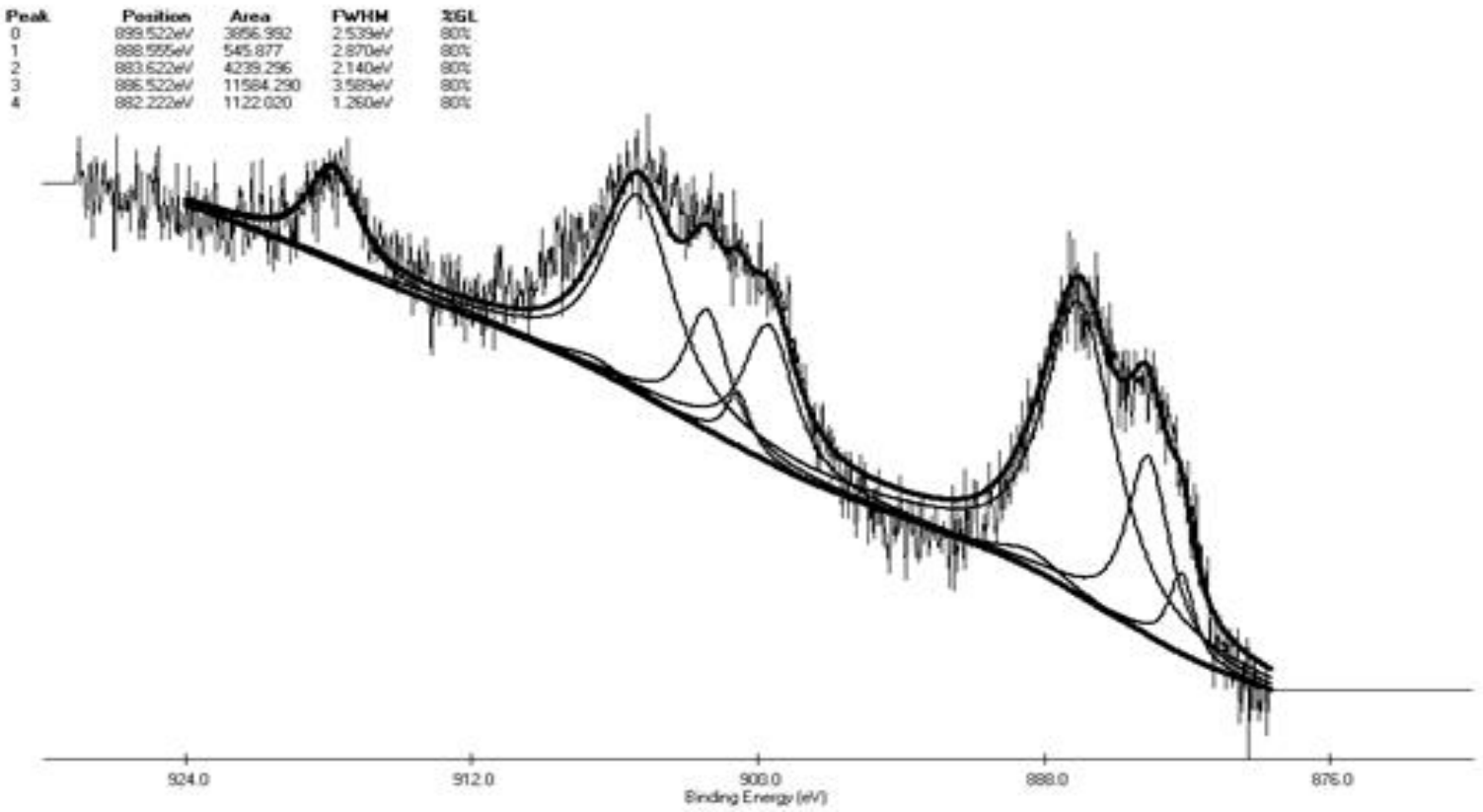

Figure 31: Binding energy spectrum for 3d orbital of Ce^{3+} nanoparticles
Similar methodology as that for Figure 27 was adopted.

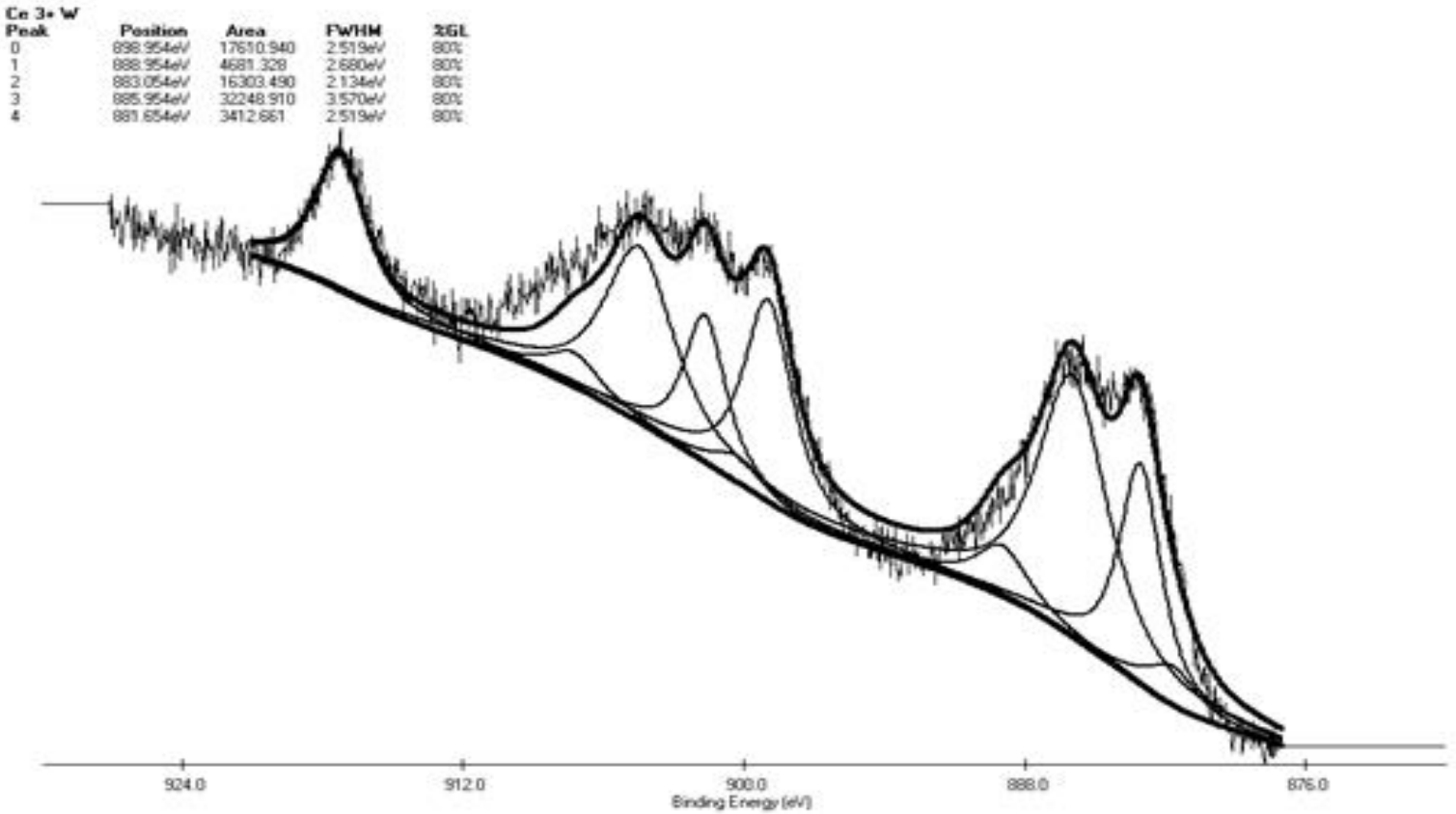

Figure 32: Tungstate significantly alters the binding energy spectrum for 3+ nanoparticles
Similar methodology as that for Figure 27 was adopted. Equimolar concentration of tungstate was mixed with nanoparticle solution and applied to a silicon wafer.

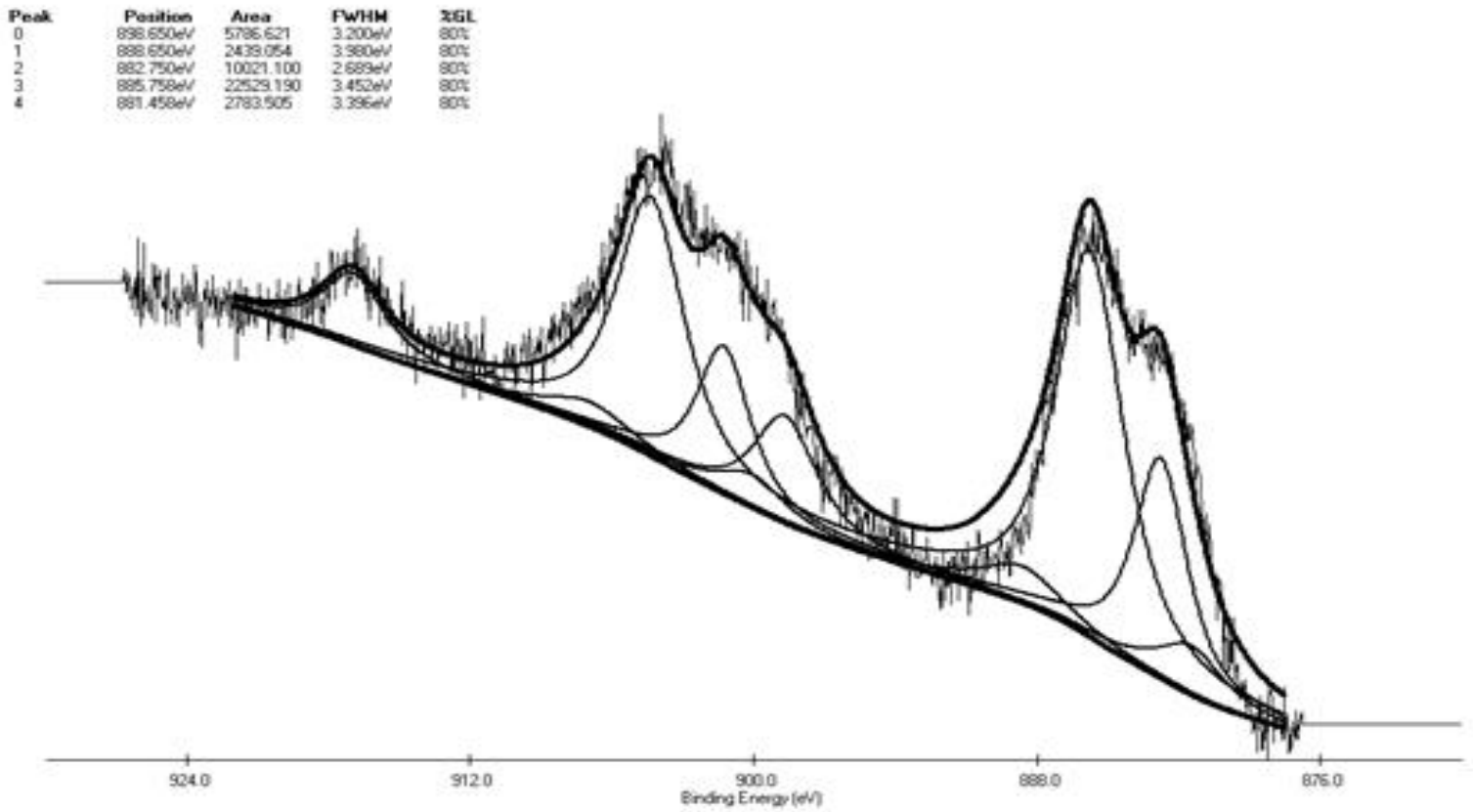

Figure 33: Molybdate does not significantly alter the binding energy spectrum for 3+ nanoparticles
Similar methodology as that for Figure 27 was adopted. Equimolar concentration of molybdate was mixed with nanoparticle solution and applied to a silicon wafer.

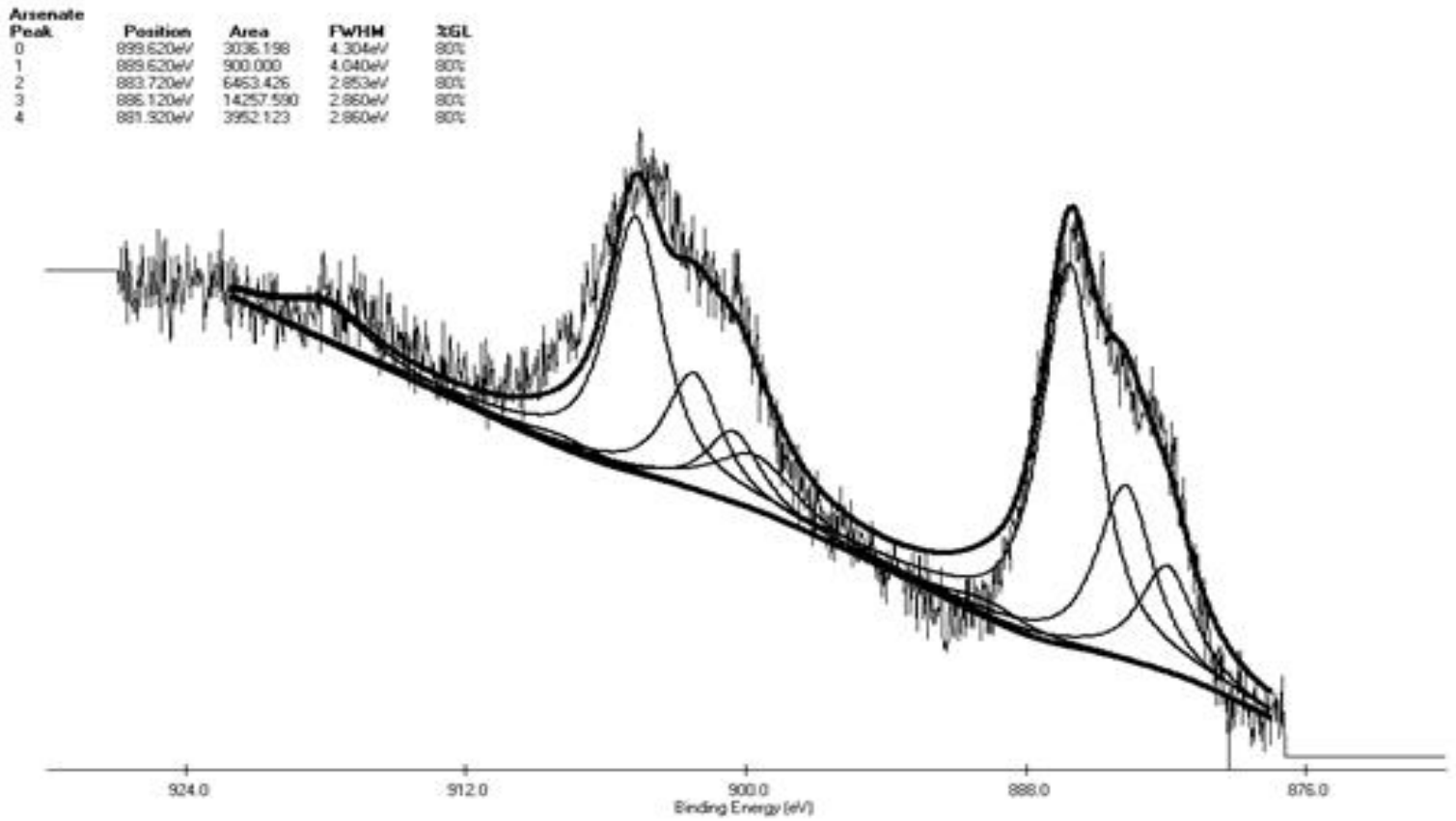

Figure 34: Arsenate significantly alters the binding energy spectrum for 3+ nanoparticles
Similar methodology as that for Figure 27 was adopted. Equimolar concentration of arsenate was mixed with nanoparticle solution and applied to a silicon wafer.

Table 5 lists the concentration of cerium atoms in the 3+ state on the nanoparticle samples that were used in the XPS experiments.

Table 5: Concentration of Ce^{3+} in nanoceria samples with and without inhibitors

		Concentration of Ce^{3+} in sample (%)			
		Control	Tungstate	Molybdate	Arsenate
Predominant state	3+	59.5	48.0	58.1	63.6
	4+	24.9	25.2	23.0	21.4

Ce^{3+} concentration changed significantly in the presence of arsenate for both 3+ and 4+ nanoparticles. The values for other inhibitors remained roughly the same except for tungstate with 3+ nanoparticles. These results suggest that for the purposes of studying phosphatase activity there is no significant change in the state of 4+ cerium oxide nanoparticles when exposed to inhibitors. Spectra for binding energy of cerium electrons in the 3d orbital with j values of 5/2 and 3/2 were used a comparison to ensure that the results obtained were not anomalous.

CONCLUSION

The goal of this project was to study the phosphatase activity of cerium oxide nanoparticles and find ways of controlling it. Cerium atoms that are in the 4+ state allow the hydrolytic cleavage of phosphate anion from donor substrates. Those in the 3+ state do not show this activity. This was confirmed by absorbance, for pNPP and ATP and by fluorescence for an alternate substrate, MUP. Water was found to play an essential role in the catalytic reaction – based on reactions using either pNPP or MUP. Their phosphatase activity is weak when compared to biological phosphatases.

Anions that are similar in structure to phosphate are able to inhibit the phosphatase mimetic activity in a dose dependent manner. Tungstate, molybdate and arsenate inhibition data were fit to a partial mixed inhibition model. It is likely that all three anions were efficient in binding to the cerium oxide nanoparticles and blocking reactive sites that would have otherwise been occupied by phosphate anions. The fact that they fit a mixed model of inhibition implies that the inhibitors can bind to both the nanoparticles and a nanoparticle-phosphate complex with varying affinities. Since there is no reason to doubt that a nanoparticle-phosphate-inhibitor complex can also lead to free phosphate, the model makes most sense when classified as partial mixed inhibition. On the whole, tungstate and molybdate seem to follow an inhibition model that is almost full ($\beta \rightarrow 0$) while arsenate inhibition is essentially leaky ($\beta > 0$). Molybdate inhibition is quite close to a special case of mixed inhibition when $\alpha = 1$ (Non-competitive Inhibition) while the values of α for tungstate and arsenate are well above 0.

Since cerium oxide nanoparticles are established scavengers of reactive oxygen and nitrogen species, it is useful to study other catalytic activities (such as phosphatase activity) that will qualify their biomedical applications by rendering information on parameters such as bioavailability and toxicity. We have used phosphatase activity as a model catalytic activity because it is easy to follow and the trend for 4+ cerium oxide nanoparticles can be quickly correlated to catalase activity.

APPENDIX
COPYRIGHT PERMISSION LETTER

The following is a notice of confirmation for permission to use Figure 4.

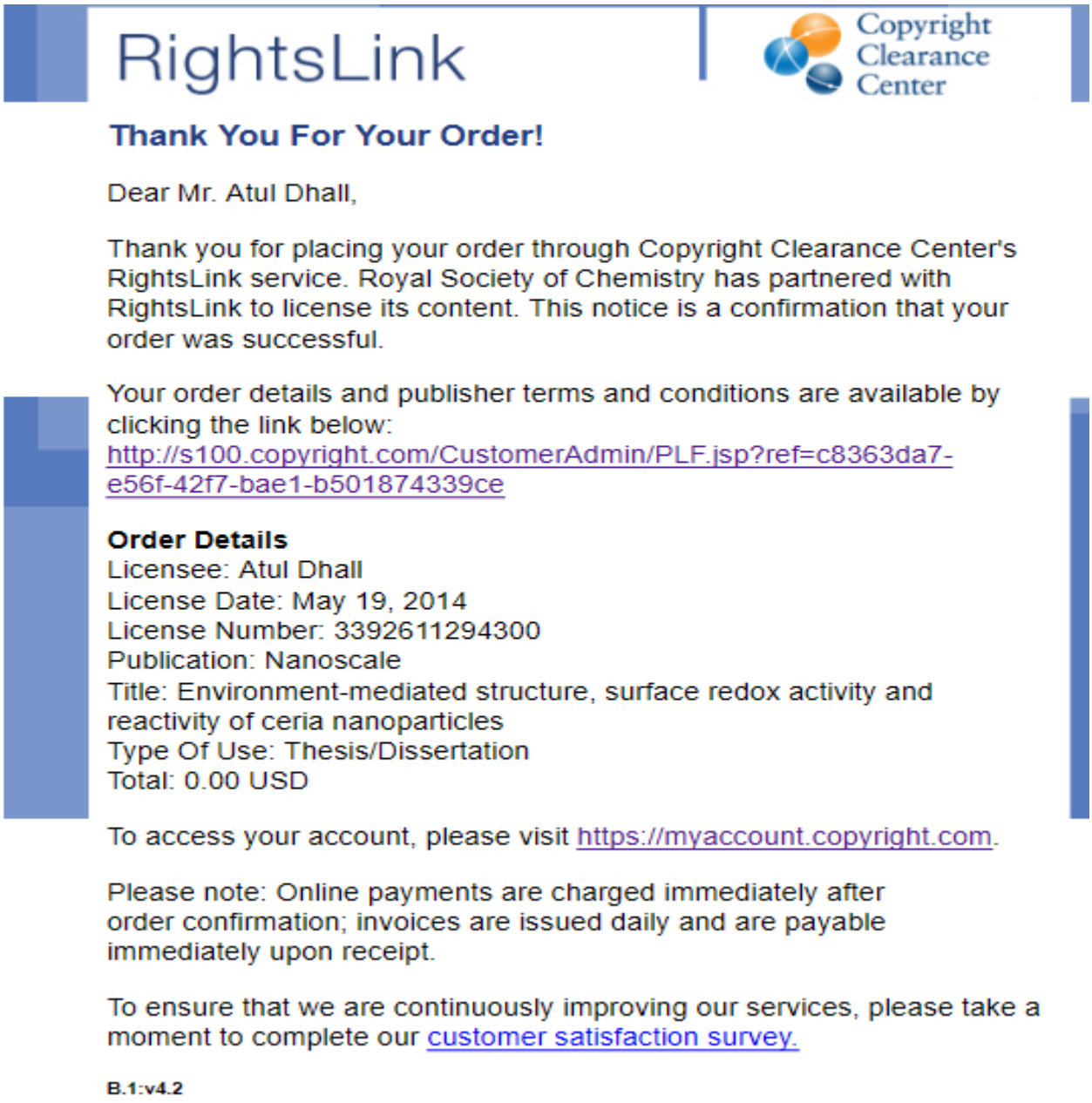

RightsLink

Copyright Clearance Center

Thank You For Your Order!

Dear Mr. Atul Dhall,

Thank you for placing your order through Copyright Clearance Center's RightsLink service. Royal Society of Chemistry has partnered with RightsLink to license its content. This notice is a confirmation that your order was successful.

Your order details and publisher terms and conditions are available by clicking the link below:
http://s100.copyright.com/CustomerAdmin/PLF.jsp?ref=c8363da7-e56f-42f7-bae1-b501874339ce

Order Details
Licensee: Atul Dhall
License Date: May 19, 2014
License Number: 3392611294300
Publication: Nanoscale
Title: Environment-mediated structure, surface redox activity and reactivity of ceria nanoparticles
Type Of Use: Thesis/Dissertation
Total: 0.00 USD

To access your account, please visit https://myaccount.copyright.com.

Please note: Online payments are charged immediately after order confirmation; invoices are issued daily and are payable immediately upon receipt.

To ensure that we are continuously improving our services, please take a moment to complete our customer satisfaction survey.

B.1:v4.2

REFERENCES

Reports and Journals

[1] NSTC. National Nanotechnology Initiative: Leading to the Next Industrial Revolution. A Report by the Interagency Working Group on Nanoscience, Engineering and Technology Committee on Technology, National Science and Technology Council, Washington, D.C. February 2000.

[2] Buettner KM, Rinciog CI, Mylon SE. Aggregation kinetics of cerium oxide nanoparticles in monovalent and divalent electrolytes. Colloids and Surfaces A: Physicochemical and Engineering Aspects. 2010;366:74-9.

[3] Gritschneder S, Reichling M. Structural elements of CeO2(111) surfaces. Nanotechnology. 2007;18:044024.

[4] Gritschneder S, Iwasawa Y, Reichling M. Strong adhesion of water to CeO2(111). Nanotechnology. 2007;18:044025.

[5] Dowding JM, Das S, Kumar A, Dosani T, McCormack R, Gupta A, et al. Cellular Interaction and Toxicity Depend on Physicochemical Properties and Surface Modification of Redox-Active Nanomaterials. ACS Nano. 2013;7:4855-68.

[6] Dutta P, Pal S, Seehra MS, Shi Y, Eyring EM, Ernst RD. Concentration of Ce3+ and Oxygen Vacancies in cerium oxide nanoparticles. Chem Mater 2006;18:5144-6.

[7] Sayle TX, Molinari M, Das S, Bhatta UM, Mobus G, Parker SC, et al. Environment-mediated structure, surface redox activity and reactivity of ceria nanoparticles. Nanoscale. 2013;5:6063-73.

[8] Dowding JM, Dosani T, Kumar A, Seal S, Self WT. Cerium oxide nanoparticles scavenge nitric oxide radical ([radical dot]NO). Chemical Communications. 2012;48:4896-8.

[9] Korsvik C, Patil S, Seal S, Self WT. Superoxide dismutase mimetic properties exhibited by vacancy engineered ceria nanoparticles. Chemical Communications. 2007;0:1056-8.

[10] Karakoti A, Singh S, Dowding JM, Seal S, Self WT. Redox-active radical scavenging nanomaterials. Chemical Society Reviews. 2010;39:4422-32.

[11] Dowding JM, Seal S, Self WT. Cerium oxide nanoparticles accelerate the decay of peroxynitrite (ONOO−). Drug Delivery and Translational Research. 2013;3:375-9.

[12] Pirmohamed T, Dowding JM, Singh S, Wasserman B, Heckert E, Karakoti AS, et al. Nanoceria exhibit redox state-dependent catalase mimetic activity. Chemical Communications. 2010;46:2736-8.

[13] Xue Y, Zhai Y, Zhou K, Wang L, Tan H, Luan Q, et al. The vital role of buffer anions in the antioxidant activity of CeO2 nanoparticles. Chemistry. 2012;18:11115-22.

[14] Singh S, Dosani T, Karakoti AS, Kumar A, Seal S, Self WT. A phosphate-dependent shift in redox state of cerium oxide nanoparticles and its effects on catalytic properties. Biomaterials. 2011;32:6745-53.

[15] Li K, Chen Y. Effect of natural organic matter on the aggregation kinetics of CeO2 nanoparticles in KCl and CaCl2 solutions: measurements and modeling. Journal of hazardous materials. 2012;209-210:264-70.

[16] Karakoti AS, Das S, Thevuthasan S, Seal S. PEGylated inorganic nanoparticles. Angewandte Chemie. 2011;50:1980-94.

[17] Das S, Singh S, Dowding JM, Oommen S, Kumar A, Sayle TX, et al. The induction of angiogenesis by cerium oxide nanoparticles through the modulation of oxygen in intracellular environments. Biomaterials. 2012;33:7746-55.

[18] Karakoti AS, Tsigkou O, Yue S, Lee PD, Stevens MM, Jones JR, et al. Rare earth oxides as nanoadditives in 3-D nanocomposite scaffolds for bone regeneration. Journal of Materials Chemistry. 2010;20:8912-9.

[19] Lin W, Huang YW, Zhou XD, Ma Y. Toxicity of cerium oxide nanoparticles in human lung cancer cells. International journal of toxicology. 2006;25:451-7.

[20] Feng X, Sayle DC, Wang ZL, Paras MS, Santora B, Sutorik AC, et al. Converting ceria polyhedral nanoparticles into single-crystal nanospheres. Science. 2006;312:1504-8.

[21] Suphantharida P, Osseo-Asare K. Cerium Oxide Slurries in CMP. Electrophoretic Mobility and Adsorption Investigations of Ceria/Silicate Interaction. Journal of The Electrochemical Society. 2004;151:G658.

[22] Campbell CT. Oxygen Vacancies and Catalysis on Ceria Surfaces. Science. 2005;309:713-4.

[23] Sun C, Li H, Chen L. Nanostructured ceria-based materials: synthesis, properties, and applications. Energy & Environmental Science. 2012;5:8475-505.

[24] Feng Z, Qiang Jin J, Siu-Wai C. Ceria nanoparticles: Size, size distribution, and shape. Journal of Applied Physics. 2004;95:4319-26.

Web-based Sources

Schematic for X-ray Photoelectron Spectroscopy
http://en.wikipedia.org/wiki/X-ray_photoelectron_spectroscopy#mediaviewer/File:System2.gif

3D lattice structure of Cerium oxide
http://en.wikipedia.org/wiki/File:Ceria-3D-ionic.png